Rheol Acta (2009) 48:779–800
DOI 10.1007/s00397-009-0372-x

ORIGINAL CONTRIBUTION

Effect of random longitudinal vibrations on the Poiseuille flow of a complex liquid

E. Emilio Herrera · F. Calderas · A. E. Chávez · O. Manero · B. Mena

Received: 3 March 2009 / Accepted: 7 June 2009 / Published online: 14 July 2009

Abstract In this work, the rectilinear Poiseuille flow of a complex liquid flowing in a vibrating pipe is analyzed. The pipe wall performs oscillations of small amplitude that can be adequately represented by a weakly stochastic process, for which a quasi-static perturbation solution scheme is suggested. The flow is analyzed using the Bautista–Manero–Puig constitutive equation, consisting on the upper-convected Maxwell equation coupled to a kinetic equation to account for the breakdown and reformation of the fluid structure. A drastic enhancement of the volumetric flow is predicted in the region where the fluid experiences pronounced shear-thinning. Finally, flow enhancement is predicted using experimental data reported elsewhere for wormlike micellar solutions of cetyl trimethyl ammonium tosilate.

E. E. Herrera (✉) · F. Calderas · A. E. Chávez
Departamento de Ingeniería Química, Facultad de Química,
Universidad Nacional Autónoma de México,
Mexico DF, 04510, Mexico
e-mail: emilio_ed@hotmail.com

A. E. Chávez
e-mail: angelenc@unam.mx

O. Manero
Departamento de Reología y Mecánica de Materiales,
Instituto de Investigaciones en Materiales,
Universidad Nacional Autónoma de México,
Mexico DF, 04510, Mexico

B. Mena
Departamento de Mecánica y Energía,
Instituto de Ingeniería,
Universidad Nacional Autónoma de México,
Mexico DF, 04510, Mexico

Keywords Vibrating pipe · Poiseuille flow · Wormlike micelles · Viscoelastic properties · Rheological modeling

Introduction

In the past, attention has been given to the flow of non-Newtonian liquids through pipes of circular cross-section generated by a pressure gradient that oscillates around a mean non-zero value. Theoretical predictions using perturbation methods on viscometric flows (or nearly viscometric flows) of the flow enhancement as a function of frequency and amplitude of oscillations have been reported (Fredrickson 1964; Barnes et al. 1969, 1971; Edwards et al. 1972; Gianetto et al. 1973; Sundstrom and Kaufman 1977; Manero and Mena 1977; Manero and Walters 1980; Kazakia and Rivlin 1978, 1979; Davies et al. 1978; Mena et al. 1979; Phan-Thien 1978, 1980a, b, 1981, 1982; Phan-Thien and Dudek 1982a, b; Mori et al. 1984; Khabakhpasheva et al. 1989; De Andrade Lima and Rey 2005, 2006; Bird et al. 1977; Herrera-Velarde and Mena 2000, 2001; Herrera-Velarde et al. 2003).

They include analytical approximations and numerical solutions of the equation of motion using several constitutive equations, namely, Maxwell, generalized Maxwell, generalized Newtonian, Bingham, Power law, Ellis, Carreau Yasuda, Tanner, White–Metzner, four-constant Oldroyd, Goddard–Miller, Wagner, B-KBKZ, Filbey–Ericksen–Criminale, and MacDonald–Bird–Carreau (Fredrickson 1964; Townsend 1973, Phan-Thien 1978, 1980a, b, 1982; Phan-Thien and Dudek 1982a, b; Bird et al. 1977; Barnes et al. 1969, 1971; Davies et al. 1978).

Previous works showed that the flow enhancement is related to the shear-thinning properties of the fluid and its magnitude depends strongly on the shape of the viscosity function. The resonance curves reported by several authors can be explained by a coupling of the viscoelastic properties with the macroscopic perturbed motion. Among them are the shape of the viscosity curve and the inter-relation of the characteristic times of the system (Manero and Walters 1980; Phan-Thien 1978, 1980a, b, 1981, 1982; Phan-Thien and Dudek 1982a, b).

In addition, it has been shown that inertia is not the dominant mechanism and that elasticity plays a secondary role in the flow enhancement (Davies et al. 1978). For viscoelastic materials, it was found that the flow enhancement depends strongly on the square of the amplitude of the oscillating pressure gradient. Nevertheless, as pointed out in several experimental studies, larger magnitudes of the flow enhancement are obtained under a constant pressure gradient with an oscillatory motion of the boundaries (Manero and Mena 1977; Kazakia and Rivlin 1978, 1979; Mena et al. 1979; Manero and Walters 1980; Phan-Thien 1980a, b; Mori et al. 1984; Khabakhpasheva et al. 1989).

Manero and Mena (1977) studied the flow without restrictions of amplitude or frequency of the oscillations. Experimental results show that the superimposed oscillations on the boundaries produce an increase in the flow, and the magnitude of this enhancement is a function of the amplitude and the frequency of the oscillations.

In addition, Kazakia and Rivlin (1978, 1979), using a perturbation technique for a slightly non-Newtonian fluid, showed that inertia is an important mechanism behind the flow enhancement, although predictions cannot match the large increments in the flow observed by Manero and Mena (1977).

Mena et al. (1979) showed that a longitudinal vibration of the pipe wall can have a strong effect on the Poiseuille flow in non-Newtonian fluids. These effects are a function of the shear-thinning behavior, viscoelastic properties, and amplitude of the superimposed oscillations, and elasticity only plays a secondary role in the flow enhancement. One way to evaluate the flow enhancement effect is the following equation: $I = \frac{Q_{osc} - Q_{stat}}{Q_{stat}}$, where Q_{osc} and Q_{stat} are the volumetric flows corresponding to the oscillatory and stationary (Poiseuille) conditions, respectively. Experiments demonstrate that a positive flow enhancement is attainable.

Phan-Thien (1980a, b) studied the problem of a fluid driven by a constant pressure gradient with random stationary oscillations of the wall with a stochastic perturbation scheme. Three constitutive equations were analyzed, namely, generalized Newtonian, strain rate, and strain-dependent constitutive equations. He found that these equations were able to describe the flow enhancement phenomenon observed by Mena et al. (1979) and that this effect was entirely associated to the interplay of inertia and the shear-thinning properties of the fluid. It was also found that a maximum in the resonance curves is determined by the coupling between the macroscopic perturbations and the viscoelastic properties of the fluid.

The interesting effects observed by Manero and Mena (1977) and Mena et al. (1979) exhibited by the flow of viscoelastic solutions through oscillating pipes suggest numerous possibilities for industrial applications in the processing of polymer melts.

For example, some of the industrial applications of the oscillating flow are in the polymer processing area (Middleman 1977), e.g., extrusion using oscillatory dies (Casulli et al. 1990; Herrera-Velarde and Mena 2000, 2001; Herrera Velarde et al. 2003). More recently, Isayev et al. (1990) and Wong et al. (1990) studied theoretically and experimentally the effects of oscillating the extruder die at high frequencies, in a polymer melt process including non-isothermal effects. Their results show the influence of the oscillation of the mean temperature of the extrudate. For the non-isothermal case, they detect an increasing temperature in the melt resulting from the oscillations; the viscous dissipation resulting from the oscillations is larger than that caused only by the pressure gradient across the die for the case of large amplitude oscillations and the conduction of heat dominates for the case of low mass flow. More recent studies consider the effects of oscillations on the heat transfer (Dunwoody 1996; Ding et al. 1999) who examined the inertial effects on the viscous dissipation under oscillations. In addition, Herrera-Velarde et al. (2003) studied the temperature rise due to viscous dissipation in oscillatory pipe flow with non-Newtonian fluids. Their results showed that the bulk temperature of the fluid at the exit of the oscillating section increases with the oscillating frequency and amplitude.

Complex fluids have been used in enhanced oil recovery operations, especially those related to underground formations. The extraction of additional amounts of oil can be achieved by hydraulically inducing fractures in the rock formations. Water-based fracturing fluids have been obtained using high molecular weight water-soluble polymers. Recently, polymer-free fracturing fluids, based on viscoelastic surfactants, have been developed for fracturing underground formations.

Fluids made of viscoelastic surfactants may provide improved fracture conductivity in comparison to polymer-based fluids.

Viscoelastic surfactants are characterized by an entangled network of large wormlike micelle structures. These structures break and reform during flow, exhibiting variable and rich rheological behavior. Predictions of the flow behavior of viscoelastic surfactants by constitutive equations have been a challenging issue (Cates 1987; Cates and Candau 1990). These systems exhibit Maxwell-type behavior in small-amplitude oscillatory shear flow and saturation of the shear stress in steady simple shear, which leads to shear banding flow (Spenley et al. 1993, 1996; Spenley and Cates 1994). In the non-linear viscoelastic regime, elongated micellar solutions also exhibit remarkable features, such as the presence of a stress plateau in steady shear flow past a critical shear rate accompanied by slow transients to reach steady state (Berret 1997).

In view of the potential technological applications, it is surprising that the rheological modeling of complex fluids, such as viscoelastic surfactants (or wormlike micellar systems) in oscillating flow, has not been treated amply in the current literature. The main objectives of this work are:

1. Predictions of the flow enhancement generated by a longitudinal vibration of the pipe wall of a complex liquid using the Bautista–Manero–Puig (BMP) constitutive equation. This equation couples a time-dependent equation for the structure changes with the upper-convected Maxwell constitutive equation. The evolution equation for the structural changes was conceived to account for the kinetic process of breakage and reformation of the micelles under flow (Bautista et al. 1999, 2000, 2002; Manero et al. 2002; Soltero et al. 1999).
2. Solution of the momentum and constitutive equations with a perturbation stochastic technique when the longitudinal vibration of the pipe wall is represented by a stochastic random function $n(t)$.
3. Characterization of the role of the kinetics, structural and viscoelastic mechanisms on the flow enhancement through dimensionless groups.
4. Use of rheometric data of an aqueous wormlike micellar solution (cetyl-trimethyl ammonium tosilate) to calculate the flow enhancement for various concentrations.

This paper is organized as follows: "Introduction" contains the introduction to the problem and previous work. "Constitutive equation (BMP model)" presents the BMP model (mathematical and physical properties). The formulation to the problem is presented in "Problem formulation", with the non-dimensional variables and the stochastic properties of the random function $n(t)$ used to describe the longitudinal vibration of the pipe wall. In the fourth section, the perturbation solution is proposed and analytical results are shown in the fifth section. Particular asymptotic results for the flow enhancement are described in "Particular and asymptotic cases". Discussion of the results, conclusion remarks and proposed future work are exposed in the last sections.

Constitutive equation (BMP model)

The BMP (Bautista et al. 1999) model is defined by the following equations:

$$\underline{\underline{\sigma}} + \frac{\eta\left(\mathrm{II}_{\underline{\underline{D}}}\right)}{G_0}\overset{\nabla}{\underline{\underline{\sigma}}} = 2\eta\left(\mathrm{II}_{\underline{\underline{D}}}\right)\underline{\underline{D}} \tag{1}$$

$$\frac{1}{\eta\left(\mathrm{II}_{\underline{\underline{D}}}\right)}\frac{d\eta\left(\mathrm{II}_{\underline{\underline{D}}}\right)}{dt} = \frac{1}{\lambda}\left(1 - \frac{\eta\left(\mathrm{II}_{\underline{\underline{D}}}\right)}{\eta_0}\right) + k\left(1 - \frac{\eta\left(\mathrm{II}_{\underline{\underline{D}}}\right)}{\eta_\infty}\right)\underline{\underline{\sigma}} : \underline{\underline{D}} \tag{2}$$

where

$$\overset{\nabla}{\underline{\underline{\sigma}}} = \frac{D}{Dt}\underline{\underline{\sigma}} - \left(\underline{\underline{\sigma}}\cdot\nabla\underline{V} + \left(\nabla\underline{V}\right)^T\cdot\underline{\underline{\sigma}}\right) \tag{3}$$

$$\frac{D}{Dt}\underline{\underline{\sigma}} = \left(\frac{\partial}{\partial t} + \underline{V}\cdot\nabla\right)\underline{\underline{\sigma}} \tag{4}$$

$$\underline{\underline{D}} = \frac{1}{2}\left(\nabla\underline{V} + \left(\nabla\underline{V}\right)^T\right) \tag{5}$$

$$\mathrm{II}_{\underline{\underline{D}}} = \sqrt{2\left(\underline{\underline{D}} : \underline{\underline{D}}\right)} \tag{6}$$

In Eq. 1 the stress $\underline{\underline{\sigma}}$ is a viscoelastic stress tensor, $\overset{\nabla}{\underline{\underline{\sigma}}}$ is the upper-convected derivative of the stress tensor given by Eq. 3, η is the viscosity function, and $\underline{\underline{D}}$ is the rate of deformation tensor, which is the symmetric part of the velocity gradient tensor (Eq. 5), $\mathrm{II}_{\underline{\underline{D}}}$ is the second invariant of the rate of deformation tensor given by Eq. 6, G_0 is the elastic modulus (Eq. 1), and finally, $\nabla\underline{V}$, $\left(\nabla\underline{V}\right)^T$ are the velocity gradient and its transpose,

respectively (Eq. 5). In Eq. 2, η_0 and η_∞ are the viscosities at zero and very high shear rates, respectively, λ is the structural relaxation time and k can be interpreted as a kinetic constant for the structure breakdown. The BMP model was selected for this study due to its capacity of predicting the thixotropic behavior of structured fluids, like wormlike micellar solutions, dispersions of lamellar liquid crystals, bentonite suspensions (Bautista et al. 1999), and polymer nanocomposites (Calderas et al. 2009) apart from reproducing the complete flow curve for a shear thinning fluid, i.e., Newtonian plateau at low and high shear rate, and the intermediate power law region (Bautista et al. 1999). Analytical solutions for the simple shear flow are obtained by using this model due to its simplicity as compared to more complex models (Acierno et al. 1976; De Kee et al. 1994; Giesekus 1966, 1982, 1984, 1985). Furthermore, all five parameters of the model are related to the fluid properties and can be estimated from rheological experiments in steady and unsteady state (Bautista et al. 1999).

Problem formulation

A schematic diagram of a problem under consideration is shown in Fig. 1. The isothermal rectilinear flow of an incompressible complex liquid under a constant pressure gradient is analyzed in a circular pipe of radius $r = a$ and axial longitude $z = L$. Entry and exit effects and gravitational forces are neglected. In this system, all physical quantities in cylindrical coordinates (r, θ, z) are defined with respect to an origin at the pipe centre. The axial velocity is a function of the spatial and temporal variables r and t, respectively, i.e., $V_z\ (r, t)$. The condition for a random longitudinal vibration at the wall is $[V_z\ (r = a,t) = \omega a n(t)]$, where $n(t)$ is a fluctuation (noise) when the pipe wall is executing a random longitudinal vibration.

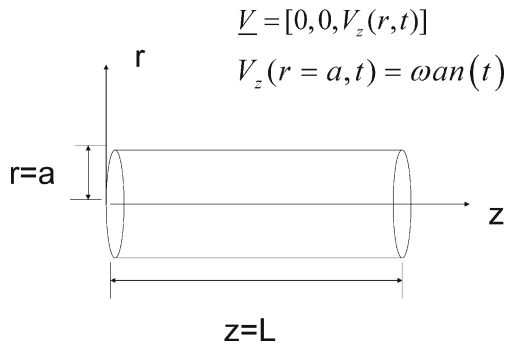

Fig. 1 Schematic representation when the pipe wall executes a random longitudinal vibration

Dimensionless variables, groups, and equations

Non-dimensional variables

To simplify the momentum and rheological equations, we introduce the following dimensionless variables for the axial velocity, pressure gradient, time, shear stress, first and second normal stress differences, shear rate, radial coordinate, viscosity function, and frequency, respectively.

$$V_z^* = \frac{V_z}{\omega a};\ p = \frac{\frac{dP}{dz}}{\frac{\eta_0}{a\lambda}};\ t^* = \frac{t}{\lambda};\ \tau = \frac{\sigma_{RZ}}{\eta_0/\lambda};$$

$$N_{(1)}^* = \frac{N_1}{\eta_0/\lambda} = \frac{\sigma_{RR} - \sigma_{\Theta\Theta}}{\eta_0/\lambda}$$

$$N_{(2)}^* = \frac{N_2}{\eta_0/\lambda} = \frac{\sigma_{\Theta\Theta} - \sigma_{ZZ}}{\eta_0/\lambda};\ \dot{\gamma}^* = \lambda\,\dot{\gamma}_{rz};\ r^* = \frac{R}{a};$$

$$\eta^* = \frac{\eta}{\eta_0};\ \omega^* = \omega\lambda \tag{7}$$

In the system of equations, the characteristic time is λ (structural build-up time). This election of the non-dimensional variables enables the comparison of this time with other characteristic times associated with the physical mechanism (e.g., viscoelastic $\lambda_0 = \eta_0 G_0^{-1}$, $\lambda_\infty = \eta_\infty G_0^{-1}$ and rupture $\lambda_r = k\eta_0$ times).

Non-dimensional groups

Using Eq. 7, the non-dimensionless components of the momentum equation, constitutive equations, and the flow enhancement are obtained. In addition, we define the following non-dimensional groups:

$$Re = \frac{\rho\,(\omega a)\,a}{\eta_0};\ De = \frac{\eta_0/G_0}{\lambda};\ A = \frac{k\eta_0}{\lambda};$$

$$B = \frac{\eta_0}{\eta_\infty};\ C = (AB)^{1/2} = \left(\frac{k\eta_0}{\lambda}\frac{\eta_0}{\eta_\infty}\right)^{1/2} \tag{8}$$

The pulsating Reynolds number (Re) (Mena et al. 1979) relates the inertial and viscous forces in the fluid. The second group is the Deborah number (De), which represents the relation between two characteristic times, the Maxwell relaxation time (which is associated to the viscoelastic properties of the fluid $\lambda_0 = \eta_0 G_0^{-1}$), and the structure relaxation time (which is a structure buildup time λ). When $De > 1$, the Maxwell time is larger than the structure time, and the fluid structure recovers faster than the rupture caused by the flow. Bautista et al. (1999) showed that, when the structural time is larger than the Maxwell time, thixotropic loops

are predicted, since the structure of the fluid does not recover during the deformation period, i.e., destruction of the structure is faster than recovery. The third non-dimensional number (A) is a relationship between the kinetic and viscous processes for structure breakdown (destruction function) and the structural recovery time λ. This dimensionless relationship can be interpreted as a ratio between two characteristic times. One is the rupture time $\lambda_r = k\eta_0$ and the other one is the structural build-up time λ. In particular, if the kinetic constant takes the value $k = G_0^{-1}$, the dimensionless number A reduces to the Deborah number, i.e., $A = De = \frac{\lambda_0}{\lambda}$, which is a measure of the magnitude and shape of the thixotropic loops in the system, so the Deborah number is a particular case of the non-dimensional number A, i.e., $De \in A$. The fourth group (B) is the ratio of the viscosities at low and high shear rates. This group is a measure of the shear-thinning ($B > 1$) and shear-thickening ($B < 1$) behavior. In terms of the structure, shear thinning behavior can be conceived as a structure breakdown process; the system undergoes a transition from a high structured state (first Newtonian plateau) to a low structured one (second Newtonian plateau), while shear thickening can be thought of as the opposite mechanism. Finally, the last group is a product of the dimensionless numbers A and B. This group can be interpreted as the square ratio of two geometrical mean relaxation times (defined as $\lambda_r = k\eta_0$, $\lambda_0 = \eta_0 G_0^{-1}$, $\lambda_\infty = \eta_\infty G_0^{-1}$), so the dimensionless number C can be rewritten as $C = \sqrt{AB} = \frac{\lambda_G^I}{\lambda_G^{II}} = \frac{\sqrt{\lambda_r \lambda_0}}{\sqrt{\lambda \lambda_\infty}}$. The time λ_G^I is associated to the structure rupture and Maxwell times, and λ_G^{II} is related to the structural and Maxwell times at high shear rate. As particular cases, when $\lambda_r = \lambda \lambda_0 \lambda_\infty^{-1}$, the dimensional number C reduces to the dimensional number B, which is a measure of the shear-thinning or shear-thickening properties of the fluid. Similarly, when $\lambda_r = \lambda_\infty \lambda_0 \lambda^{-1}$, the equality $C = De$ is obtained. It is important to note that when $C > 1$, the rupture and viscoelastic relaxation times dominate over the structural and Maxwell (at high shear rates) times. In contrast, when $C < 1$, the effects of the structural and Maxwell times (at high shear rates) are the dominating mechanisms. Moreover, the effects of thixotropy are included as particular cases when $k = G_0^{-1}$. These quantities satisfy the inequality $De \leq C \leq B$.

Non-dimensional momentum equation

$$Re \frac{\partial V_z^* (r^*, t^*)}{\partial t^*} = -p + \frac{1}{r^*} \frac{\partial}{\partial r^*} \left(r^* \tau \left(r^*, t^* \right) \right) \tag{9}$$

and the non-dimensional boundary conditions

$$V_z^* \left(r^* = 1, t^* \right) = n \left(t^* \right) \tag{10}$$

$$\overset{\bullet}{\gamma}{}^* \left(0, t^* \right) = \frac{\partial}{\partial r^*} V_z^* \left(r^*, t^* \right) \Big|_{r^*=0} = 0 \tag{11}$$

Notice that, in Eq. 10, $n(t^*)$ is a stochastic dimensionless random stationary function.

Non-dimensional BMP equation of state

$$\left(1 + De\eta^* \left(\overset{\bullet}{\gamma}{}^* \right) \frac{\partial}{\partial t^*} \right) \tau - De\eta^* \left(\overset{\bullet}{\gamma}{}^* \right) N_{(2)}^* = \eta^* \left(\overset{\bullet}{\gamma}{}^* \right) \overset{\bullet}{\gamma}{}^* \tag{12}$$

$$\left(1 + De\eta^* \left(\overset{\bullet}{\gamma}{}^* \right) \frac{\partial}{\partial t^*} \right) N_{(1)}^* = 2De\tau^2 \tag{13}$$

$$\left(1 + De\eta^* \left(\overset{\bullet}{\gamma}{}^* \right) \frac{\partial}{\partial t^*} \right) N_{(2)}^* = 0 \tag{14}$$

$$\begin{aligned} \frac{1}{\eta^* (r^*, t^*)} \frac{d\eta^* (r^*, t^*)}{dt^*} &= \left(1 - \eta^* \left(r^*, t^* \right) \right) \\ &\quad + A \left(1 - B\eta^* \left(r^*, t^* \right) \right) \\ &\quad \times \tau \left(r^*, t^* \right) \overset{\bullet}{\gamma}{}^* \left(r^*, t^* \right) \end{aligned} \tag{15}$$

Non-dimensional flow enhancement

$$I\,(\%) = 100 \frac{\int_0^1 \left(\left\langle \overset{\bullet}{\gamma}{}^* (r^*, t^*) \right\rangle - \overset{\bullet}{\gamma}{}^*_0 (r^*) \right) r^{*2} dr^*}{\int_0^1 \overset{\bullet}{\gamma}{}^* (r^*)\, r^{*2} dr^*} \tag{16}$$

$$\left\langle \overset{\bullet}{\gamma}{}^* \left(r^*, t^* \right) \right\rangle = \frac{\int_0^{2\pi/\omega^*} \overset{\bullet}{\gamma}{}^* (r^*, t^*)\, dt^*}{\int_0^{2\pi/\omega^*} dt^*} \tag{17}$$

Previous theoretical works and experimental observations in micellar solutions, such as cetyl trimethylammonium tosylate (CTAT) and erucyl bis(hydroxyethyl) methylammonium chloride (EHAC) (and works by Soltero et al. 1999; Bautista et al. 1999, 2002), showed that the contribution of the second stress difference is small, so the third term can be neglected, i.e., $De\eta^* \left(\overset{\bullet}{\gamma}{}^* \right) N_{(2)}^* \cong 0$.

Stochastic non-dimensional random function

A non-dimensional stochastic function $n(t^*)$ is considered. It is assumed that the longitudinal vibration pipe

is given in the non-dimensional form (Eq. 10). It is important to note that the stochastic function $n(t^*)$ represents random wall oscillations of small amplitude. Analytical progress is possible if $n(t^*)$ is considered as a stationary random function of time (Yaglom 1965)

$$n\left(t^*\right) = \int_{-\infty}^{+\infty} e^{i\alpha t^*} dZ\left(\alpha\right) \tag{18}$$

where $dZ(\alpha)$ is an interval random function of α with zero mean and uncorrelated increments

$$\langle dZ\left(\alpha\right)\rangle = 0 \tag{19}$$

$$\left\langle dZ\left(\alpha_i\right) d\overline{Z}\left(\alpha_j\right)\right\rangle = \delta_{ij}\Omega\left(\alpha_i\right) d\alpha_j \tag{20}$$

here and elsewhere in the paper, $\langle\,\rangle$ denotes an ensemble average and the overbar a complex conjugate quantity. In Eq. 20, δ_{ij} is the Kronecker delta and $\Omega(\alpha_i)$ is the spectral density of $n(t^*)$ defined by:

$$\Omega\left(\alpha\right) = \frac{1}{2\pi}\int_{-\infty}^{+\infty} e^{-i\alpha s} R\left(s\right) ds \tag{21}$$

where:

$$R\left(s\right) = \overline{\langle n\left(t^*\right)} n\left(t^* + s\right)\rangle = \int_{-\infty}^{+\infty} e^{i\alpha s}\Omega\left(\alpha\right) d\alpha \tag{22}$$

In Eqs. 21 and 22, it is assumed that $|R(s)|$ tends to zero fast enough as $|s|$ tends to infinity, a condition met by most, if not all, physically realizable processes as reported by Phan-Thien (1980a, b, 1981) and by Phan-Thien and Dudek (1982a, b).

Perturbation scheme

In order to find an analytical expression for the flow enhancement, a quasi-static perturbation solution in terms of the oscillatory Reynolds number is suggested. Experimental observations and theoretical works have shown that the Reynolds number is smaller that 0.01 (Barnes et al. 1969, 1971; Mena et al. 1979; Manero and Mena 1977; Manero and Walters 1980; Davies et al. 1978; Phan-Thien 1982). The axial velocity, shear strain, shear stress, viscosity function, and first and second normal stress differences can be expressed in power series of the oscillatory Reynolds number:

$$\begin{aligned}
V_z^*\left(r^*, t^*\right) &= \left(V_{z(0)}^*\left(r^*\right) + n\left(t^*\right)\right) Re^0 \\
&\quad + \left(V_{z(1)}^*\left(r^*\right) + n\left(\dot{t}^*\right)\right) Re^1 \\
&\quad + \left(V_{z(2)}^*\left(r^*\right) + n\left(\ddot{t}^*\right)\right) Re^2 + \cdots \\
\dot{\gamma}^*\left(r^*, t^*\right) &= \dot{\gamma}_0^*\left(r^*\right) Re^0 + \dot{\gamma}_1^*\left(r^*, t^*\right) Re^1 \\
&\quad + \dot{\gamma}_2^*\left(r^*, t^*\right) Re^2 + \cdots \\
\eta^*\left(r^*, t^*\right) &= \eta_0^*\left(r^*\right) Re^0 + \left(\dot{\gamma}_1^*\left(r^*, t^*\right)\dot{\eta}_0^*\right) Re^1 \\
&\quad + \left(\dot{\gamma}_2^*\left(r^*, t^*\right)\dot{\eta}_0^* + \frac{1}{2}\dot{\gamma}_2^{*2}\left(r^*, t^*\right)\ddot{\eta}_0^*\right) Re^2 + \cdots \\
\tau\left(r^*, t^*\right) &= \tau_0\left(r^*\right) Re^0 + \left(\dot{\gamma}_1^*\left(r^*, t^*\right)\dot{\tau}_0\right) Re^1 \\
&\quad + \left(\dot{\gamma}_2^*\left(r^*, t^*\right)\dot{\tau}_0 + \frac{1}{2}\dot{\gamma}_1^{*2}\left(r^*, t^*\right)\ddot{\tau}_0\right) Re^2 + \cdots \\
N_{(1)}^*\left(r^*, t^*\right) &= N_{(1)0}^*\left(r^*\right) Re^0 + N_{(1)1}^*\left(r^*, t^*\right) Re^1 \\
&\quad + N_{(1)2}^*\left(r^*, t^*\right) Re^2 + \cdots \\
N_{(2)}^*\left(r^*, t^*\right) &= N_{(2)0}^*\left(r^*\right) Re^0 + N_{(2)1}^*\left(r^*, t^*\right) Re^1 \\
&\quad + N_{(2)2}^*\left(r^*, t^*\right) Re^2 + \cdots
\end{aligned} \tag{23}$$

In Eq. 23, $n(\dot{t}^*)$ and $n(\ddot{t}^*)$ are the first and second times derivatives of the non-dimensional stochastic function $n(t^*)$, respectively.

In order to find an analytical solution, Taylor's theorem allows to express $\tau_j(r^*,t^*)$ and $\eta^*{}_j(r^*,t^*)$ ($j \in I = \{0, 1, 2...,\}$) of Eq. 23 in terms of the derivatives of $\tau_0(r^*)$ and $\eta_0^*(r^*)$, where the following shorthand notation has been used:

$$\dot{\tau}_0 = \left.\frac{d\tau\left(\dot{\gamma}^*\right)}{d\dot{\gamma}^*}\right|_{\dot{\gamma}^* \to \dot{\gamma}_0^*(r^*)}; \qquad \ddot{\tau}_0 = \left.\frac{d^2\tau\left(\dot{\gamma}^*\right)}{d\dot{\gamma}^{*2}}\right|_{\dot{\gamma}^* \to \dot{\gamma}_0^*} \tag{24}$$

$$\dot{\eta}_0^* = \left.\frac{d\eta^*\left(\dot{\gamma}^*\right)}{d\dot{\gamma}^*}\right|_{\dot{\gamma}^* \to \dot{\gamma}_0^*}; \qquad \ddot{\eta}_0^* = \left.\frac{d^2\eta^*\left(\dot{\gamma}^*\right)}{d\dot{\gamma}^{*2}}\right|_{\dot{\gamma}^* \to \dot{\gamma}_0^*} \tag{25}$$

It is important to note that the particular perturbation expansion for the velocity is different to the other

variable expansions to simplify the inertial effects in the momentum equation (Phan-Thien 1980a, b; Herrera Velarde et al. 2003; Herrera 2009; Brown and Churchill 2001), i.e., the partial time derivative of the axial velocity.

Asymptotic analysis for small oscillatory Reynolds numbers

Zeroth-order theory

Substitution of Eqs. 23, 24, and 25 into 9–17, and 18 and equating terms of the same order in the oscillatory Reynolds number leads to the zeroth-order solution, i.e., $O(Re^0)$:

$$\tau_0 = \eta_0^* \dot{\gamma}_0^* = \tau_w r^* \tag{26}$$

$$\eta_0^* = \frac{A\dot{\gamma}_0^{*2} - 1 + \sqrt{\left(A\dot{\gamma}_0^{*2} - 1\right)^2 + 4AB\dot{\gamma}_0^{*2}}}{2AB\dot{\gamma}_0^{*2}} \tag{27}$$

$$N_{(1)0}^* = 2De\tau_0^2 \tag{28}$$

$$N_{(2)0}^* = 0 \tag{29}$$

$$I(\%) = 0 \tag{30}$$

In Eq. 26, $\tau_w = \tau_0(r = 1)$ is the wall stress, and the boundary condition $\tau_0 = 0$ at $r = 0$ has been used. Equations 27, 28, and 29 are the viscosity and first and second normal stress differences of the BMP model. According to Eq. 30, no flow enhancement to zeroth order is predicted. In the rest of the paper, the first and second normal stresses differences are not considered since they are not relevant for the calculation of the flow enhancement.

First-order theory

The following equations show the solutions to first order in the oscillatory Reynolds number, i.e., $O(Re^1)$:

$$\tau_1\left(r^*, t^*\right) = \frac{1}{2\tau_w}\tau_0 n\left(\dot{t}^*\right) \tag{31}$$

$$\dot{\gamma}_1^*\left(r^*, t^*\right) = \frac{1}{2\tau_w}\left(\frac{\tau_0}{\dot{\tau}_0}\right)\left(n\left(\dot{t}^*\right) + De\eta_0^* n\left(\ddot{t}^*\right)\right) \quad \dot{\tau}_0 \neq 0 \tag{32}$$

$$I(\%) = 100Re\frac{\int_0^1 \left\langle \dot{\gamma}_1^*\left(r^*, t^*\right)\right\rangle r^{*2} dr^*}{\int_0^1 \dot{\gamma}_0^*\left(r^*\right) r^{*2} dr^*} \tag{33}$$

In Eqs. 31 and 32, the boundary conditions $\tau_1\left(r^*, t^*\right) = \dot{\gamma}_1^*\left(r^*, t^*\right) = 0$ at $r^* = 0$ were used. The shear rate to first order satisfies the differential equation given in Appendix A. On the other hand, the average of equations (Eq. 32) is zero, i.e., $\left\langle \dot{\gamma}_1^*\left(r^*, t^*\right)\right\rangle = 0$. As a consequence, the flow enhancement (Eq. 33) to first order is again zero, i.e., $I(\%) = 0$.

Second-order theory

The second order solutions in the oscillatory Reynolds number, i.e., $O(Re^2)$, are:

$$\tau_2\left(r^*, t^*\right) = \frac{1}{2\tau_w}\tau_0 n\left(\ddot{t}^*\right) \tag{34}$$

$$\dot{\gamma}_2^*\left(r^*, t^*\right) = -\frac{1}{2}\frac{\ddot{\tau}_0}{\dot{\tau}_0}\dot{\gamma}_1^{*2}\left(r^*, t^*\right) + De\dot{\eta}_0^*\frac{\tau_0}{\dot{\tau}_0} n\left(\dot{t}^*\right)\dot{\gamma}_1^*\left(r^*, t^*\right) + \frac{\tau_0}{2\tau_w}\left(\frac{n\left(\ddot{t}^*\right) + De\eta_0^* n\left(\dddot{t}^*\right)}{\dot{\tau}_0}\right) \tag{35}$$

$$I(\%) = 100Re^2\frac{\int_0^1 \left\langle \gamma_2^*\left(r^*, t^*\right)\right\rangle r^{*2} dr^*}{\int_0^1 \gamma_0^*\left(r^*\right) r^{*2} dr^*} \tag{36}$$

$$\dot{\eta}_0^* \neq 0; \dot{\tau}_0 \neq 0$$

In Eqs. 34 and 35, the boundary conditions $\tau_2\left(r^*, t^*\right) = \dot{\gamma}_2^*\left(r^*, t^*\right) = 0$ at $r^* = 0$ were used. Notice that the shear-rate to second order (Eq. 35), satisfies the differential equation given in Appendix A.

To calculate the flow enhancement, the average value of Eq. 36 is taken. Substituting Eq. 32 into Eq. 35 and using the random stochastic definitions (Eqs. 18–21, and 22), the average shear rate to second order is obtained:

$$\left\langle \dot{\gamma}_2^*\left(r^*, t^*\right)\right\rangle = \frac{1}{2}\left(\frac{1}{2\tau_w}\right)^2 \times \tau_0^2\left\{-\frac{\ddot{\tau}_0}{\dot{\tau}_0^3}\left(R_0(0) + De^2\eta_0^{*2} R_1(0)\right) + De^2\frac{\dot{\eta}_0^{*2}}{\dot{\tau}_0^2} R_0(0)\right\} \tag{37}$$

where:

$$R_0(0) = \int_{-\infty}^{+\infty} \alpha^2 \Omega(\alpha)\, d\alpha \tag{38}$$

$$R_1(0) = \int_{-\infty}^{+\infty} \alpha^4 \Omega(\alpha)\, d\alpha \tag{39}$$

(The mathematical development of Eqs. 37, 38, and 39 is given in Appendix B).

Particular stochastic random function

Sinusoidal pressure wave form

The simplest harmonic random function is given by a sinusoidal function with frequency $\omega^* = \lambda\omega$ and amplitude M, i.e.,

$$n(t^*) = M \sin(\omega^* t^*) \tag{40}$$

the spectral density $\Omega(\alpha)$ and the correlation functions $R_0(0)$ and $R_1(0)$ are given by:

$$\Omega(\alpha) = \frac{1}{4}\left(\delta(\alpha - \omega^*) + \delta(\alpha + \omega^*)\right) \tag{41}$$

$$R_1(0) = \omega^{*2} R_0(0) \tag{42}$$

where

$$R_0(0) = \langle n(t^*)\, n(t^* + 0)\rangle = \frac{1}{2}\omega^{*2} M^2 \tag{43}$$

The election of a sinusoidal pressure wave enables the comparison with the representative theoretical works, as reported by Barnes et al. (1969, 1971), Phan-Thien (1978, 1980a, b, 1981, 1982), Phan-Thien and Dudek (1982a, b), and Bird et al. (1977). On the other hand, non-harmonic effects are included in the Fourier series proposed by Townsend (1973). Phan-Thien (1978, 1980a, b) showed that the harmonics can increase o decrease the flow enhancement depending on the particular random function $n(t^*)$.

Next, Eq. (42) is substituted into Eq. 37 and then in Eq. 36 to give

$$I(\%) = \frac{25}{4} M^2 \omega^{*2} Re^2 \frac{\int_0^1 \tau_0^2 \left(-\frac{\ddot{\tau}_0}{\dot{\tau}_0^3}\left(1 + \omega^{*2} De^2 \eta_0^{*2}\right) + \omega^{*2} De^2 \frac{\dot{\eta}_0^{*2}}{\dot{\tau}_0^2}\right) r^{*2} dr^*}{\tau_w^2 \int_0^1 \dot{\gamma}_0^*(r^*)\, r^{*2} dr^*} \tag{44}$$

To simplify the numerical integration, Eq. 44 can be expressed in terms of the wall shear rate. From Eq. 26, the shear stress to zeroth-order is $\tau_0 = \tau_w r^*$, so:

$$I(\%) = \frac{25}{4} M^2 \omega^{*2} Re^2 \frac{\int_0^{\dot{\gamma}_w^*} \tau_0^4 \left(-\frac{\ddot{\tau}_0}{\dot{\tau}_0^2}\left(1 + \omega^{*2} De^2 \eta_0^{*2}\right) + \omega^{*2} De^2 \frac{\dot{\eta}_0^{*2}}{\dot{\tau}_0}\right) d\dot{\gamma}_0^*(r^*)}{\tau_w^2 \int_0^{\dot{\gamma}_w^*} \dot{\gamma}_0^*(r^*)\, d\left(\frac{1}{3}\tau_0^3\right)} \tag{45}$$

Equation 45 can be examined in particular cases.

Changing the integration variable $u = \tau_0^4\left(1 + \omega^{*2} De^2 \eta_0^{*2}\right)$ and $dv = -\frac{\ddot{\tau}_0}{\dot{\tau}_0^2} d\dot{\gamma}_0^* = \frac{d}{d\dot{\gamma}_0^*}\left[\frac{1}{\dot{\tau}_0}\right] d\dot{\gamma}_0^* = d\left[\frac{1}{\dot{\tau}_0}\right]$ in the first integral and thereafter integrating by parts, the flow enhancement is obtained (see Appendix C)

$$I(\%) = \frac{75}{4} M^2 \omega^{*2} Re^2 \frac{\tau_w^4 - 4\dot{\tau}_w \int_0^{\dot{\gamma}_w^*} \tau_0^3 d\dot{\gamma}_0^* + We^2\left(\tau_w^4 \eta_w^{*2} - 4\dot{\tau}_w \int_0^{\dot{\gamma}_w^*} \eta_0^{*2} \tau_0^3 d\dot{\gamma}_0^*\right)}{\tau_w^2 \dot{\tau}_w \left(\dot{\gamma}_w^* \tau_w^3 - \int_0^{\dot{\gamma}_w^*} \tau_0^3 d\dot{\gamma}_0^*\right)} \tag{46}$$

In Eq. 46, $We = \omega^* De = \frac{\eta_0}{G_0}\omega$ is the pulsating Weissenberg number, which characterizes the relation between the relaxation Maxwell time and the frequency of the pulsations, and $\eta^*_w = \eta^*_0\left(\dot{\gamma}^*_w\right)$, $\tau_w = \tau_0\left(\dot{\gamma}^*_w\right)$ are the viscosity function and stress at the wall, respectively. Bird et al. (1977) used the White–Metzner model with an alternative perturbation technique and obtained a similar expression.

To solve the integrals given in Eq. 47, the following relationship between the wall shear stress and the wall shear rate in Eqs. 25 and 26 is used:

$$\dot{\gamma}^*_w(\tau_w) = \frac{AB\tau_w^2 - 1 + \sqrt{\left(AB\tau_w^2 - 1\right)^2 + 4A\tau_w^2}}{2A\tau_w} \tag{47}$$

Phan-Thien (1980a, b) obtained similar results for three different constitutive equations, the generalized Newtonian fluid and the Tanner and KBKZ models.

Flow enhancement as a function of the oscillating frequency

The flow enhancement is dependent on the dimensionless frequency, according to Eq. 46, which may be cast in the following form:

$$\mathrm{I}(\%) = \frac{75}{4} M^2\beta^2\left\{\delta_1 + \delta_2\omega^{*2}De^2\right\}\omega^{*4} \tag{48}$$

where $\beta = \frac{a^2/\lambda}{\eta_0/\rho}$ and δ_1 and δ_2 are given by:

$$\delta_1(A, B) = \tau_w^{-2}\frac{\tau_w^4 - 4\dot{\tau}_w\int_0^{\dot{\gamma}^*_w}\tau_0^3 d\dot{\gamma}^*_0}{\dot{\tau}_w\left(\dot{\gamma}^*_w\tau_w^3 - \int_0^{\dot{\gamma}^*_w}\tau_0^3 d\dot{\gamma}^*_0\right)};$$

$$\delta_2(A, B) = \tau_w^{-2}\frac{\tau_w^4\eta^{*2}_w - 4\dot{\tau}_w\int_0^{\dot{\gamma}^*_w}\eta^{*2}_0\tau_0^3 d\dot{\gamma}^*_0}{\dot{\tau}_w\left(\dot{\gamma}^*_w\tau_w^3 - \int_0^{\dot{\gamma}^*_w}\tau_0^3 d\dot{\gamma}^*_0\right)} \tag{49}$$

Equation 49 describes the flow enhancement as a function of the non-dimensional frequency when the values of δ_1 and δ_2 are fixed. It is important to note that β can be interpreted as a ratio between two diffusion coefficients. One of them is associated to the diffusive processes of the structure and the other one related to the momentum transport mechanisms. Finally δ_1 and δ_2 are ratios of integrals that may be determined for particular values of the non-dimensional numbers (A, B).

It is possible to obtain a frequency range for which both the perturbation stochastic solution technique and equations given by Eq. 46 or 48 are valid but only in the limit of sufficiently low oscillating Reynolds number, i.e., $Re << 1$, and therefore,

$$0 \le Re << 1 \Rightarrow 0 \le \beta\omega^* << 1 \Rightarrow 0 \le \omega^* << \omega^*_C = \beta^{-1} \tag{50}$$

Consequently, the critical non-dimensional frequency $\left(\omega_C = \beta^{-1}\right)$ is determined according to the ratio between structural and momentum diffusivities.

Maximum flow enhancement as a function of the oscillating frequency

An analytical solution for the maximum flow enhancement as a function of frequency can be obtained by taking the first derivative of Eq. 48 and setting the result to zero. The critical dimensionless frequency is henceforth obtained:

$$\frac{d}{d\omega^*}\left[I(\%)\right] = 0; \Rightarrow \omega^*_{\mathrm{crit}} = De^{-1}\sqrt{\frac{1}{2}\frac{\delta_1}{(-\delta_2)}}; \frac{\delta_1}{(-\delta_2)} > 0 \tag{51}$$

Taking the second derivative of Eq. 48 and substituting in the result of the critical non-dimensional frequency (Eq. 51), the following expression is obtained:

$$\frac{d^2}{d\omega^{*2}}\left[\mathrm{I}(\%)\right] = -75M^2\beta^2\delta_1 < 0 \tag{52}$$

Substituting the critical dimensionless frequency (Eq. 51) into Eq. 49, the maximum flow enhancement $I_{\max}(\%)$ as a function of the non-dimensional frequency is obtained:

$$I_{\max}(\%) = 2.34M^2\frac{\delta_1^2}{(-\delta_2)}\left(\frac{\beta}{De}\right)^2; (-\alpha_2) > 0 \tag{53}$$

Equation 53 implies that the value of the maximum flow enhancement is determined by the kinetic, structural, viscoelastic, and inertial contributions through the non-dimensional numbers (β, De) and the square of the amplitude and the particular form of the stochastic function considered.

Particular and asymptotic cases

Tanner model

Equation 46 embodies the Tanner model (TM) and generalized Newtonian models if the following identifications are made: viscosity functions $\left(\eta_w^* = \eta_0^* = 1\right)$, the viscoelastic and the structural times in the BMP model $\left(\eta_0 G_0^{-1} \cong \lambda\right)$, $\varepsilon \langle V \rangle = \omega a$, and the amplitude of the longitudinal vibration of the pipe wall $\left(M^2 = 1\right)$. In this case, Eq. 46 takes the form

$$I(\%) = \frac{75}{4}\varepsilon^2\omega^{*2}Re^2\tau_w^{-2}\frac{\tau_w^4 - 4\dot{\tau}_w\int_0^{\dot{\gamma}_w^*}\tau_0^3 d\dot{\gamma}_0^*}{\dot{\tau}_w\left(\dot{\gamma}_w^*\tau_w^3 - \int_0^{\dot{\gamma}_w^*}\tau_0^3 d\dot{\gamma}_0^*\right)}\left(1+\omega^{*2}\right) \tag{54}$$

In Eq. 54, ε is a small parameter. The above equation was deduced by Phan-Thien (1978, 1980a) using a similar scheme.

Generalized Newtonian model

Notice that Eq. 54 can be simplified to the flow enhancement expression for a generalized Newtonian fluid as reported by Phan-Thien (1980a) and by Davies et al. (1978), when the dimensionless frequency is of order one, i.e., $1 + \omega^{*2} \cong 1$. Equation 54 reduces to the inelastic case:

$$I(\%) = \frac{75}{4}\varepsilon^2\omega^{*2}Re^2\tau_w^{-2}\frac{\tau_w^4 - 4\dot{\tau}_w\int_0^{\dot{\gamma}_w^*}\tau_0^3 d\dot{\gamma}_0^*}{\dot{\tau}_w\left(\dot{\gamma}_w^*\tau_w^3 - \int_0^{\dot{\gamma}_w^*}\tau_0^3 d\dot{\gamma}_0^*\right)} \tag{55}$$

In addition, Phan-Thien (1980a, b, 1981, 1982) and Phan-Thien and Dudek (1982a, b) obtained similar results for three different constitutive equations, the strain-rate-dependent fluid and strain-dependent fluid models using a similar stochastic perturbation technique in terms of the small parameter (ε).

Inelastic effects

Equation 48 contains the following asymptotic solutions when $\delta_1 >> \omega^{*2}De^2\delta_2$:

$$\frac{I_1(\%)}{I_0(\%)} \cong \left(\frac{\omega_1^*}{\omega_0^*}\right)^4 \tag{56}$$

In Eq. 56, $I_0(\%)$ and $I_1(\%)$ are the flow enhancements for dimensional frequencies ω_0^* and ω_1^*, respectively. If $\omega_1^* = N\omega_0^*$; $\left(N \in R^+\right)$, Eq. 56 takes the form:

$$I_1(\%) \cong (N)^4 I_0(\%) \tag{57}$$

Elastic effects

The flow enhancement has the approximate form when elastic forces dominate:

$$\frac{I_1(\%)}{I_0(\%)} \cong \left(\frac{\omega_1^*}{\omega_0^*}\right)^6 \tag{58}$$

which implies that

$$I_1(\%) \cong (N)^6 I_0(\%) \tag{59}$$

Approximate solution to the flow enhancement in the shear-thinning region

In the shear-thinning region of the flow curve, the flow enhancement calculated by the BMP model has the following approximate expression when the first derivative undergoes a minimum and Eq. 48 adopts the asymptotic form of the maximum:

$$I_{\max-\text{ela}}(\%) \approx \frac{75}{4}M^2\omega^{*2}Re^2\frac{\tau_w^2\left(1 + We^2\eta_w^{*2}\right)}{\dot{\tau}_w\left(\dot{\gamma}_w^*\tau_w^3\int_0^{\dot{\gamma}_w^*}\tau_0^3 d\dot{\gamma}_0^*\right)} \tag{60}$$

The inelastic case is obtained when $1 + We^2\eta_w^{*2} \cong 1$,

$$\mathrm{I}_{\max-\text{ine}}(\%) \approx \frac{75}{4}M^2\omega^{*2}Re^2\frac{\tau_w^2}{\dot{\tau}_w\left(\dot{\gamma}_w^*\tau_w^3 - \int_0^{\dot{\gamma}_w^*}\tau_0^3 d\dot{\gamma}_0^*\right)} \tag{61}$$

Flow enhancement

The flow enhancement for the BMP model can be calculated using Eqs. 44 and 46. In these, the flow enhancement can be separated into two contributions: inelastic and elastic.

Equation 44 contains a higher order derivative of the shear stress and describes the effects of the convexity in the constitutive relationship between the shear stress and shear strain in the flow enhancement.

In contrast, Eq. 46 describes the effect of the monotonic increase of the constitutive equation through the first derivative of the shear stress (to zero order). Notice that both Eqs. 44 and 46 predict a maximum in the

region where the first derivative of the shear stress is near zero, i.e., $\dot{\tau}_0 \cong 0$ (shear-thinning zone).

According to the BMP model, the flow enhancement is a function of the square of the amplitude of the oscillations, the Reynolds number, the Weissenberg number, the dimensionless numbers A and B (representing viscoelastic, kinetic and structural effects).

The maximum flow enhancement is a function of the frequency and depends on the structural properties, diffusive coefficients, and wave pressure form as given by Eq. 53.

Asymptotic results

When the elastic effects are neglected (e.g., micellar system as EHAC and CTAT), Eqs. 55 and 56 relate the flow enhancement and the non-dimensional frequency, for sufficiently small frequencies.

Using rheometric data, in the region of maximum shear thinning (where the system undergoes a structural transition), the largest flow enhancement can be obtained using Eqs. 60 and 61 in the elastic and inelastic cases, respectively.

Results

BMP theoretical predictions

The flow enhancement integral Eq. 46 was solved numerically by using a quadrature Gaussian method combined with a Lagrange method to extrapolate to zero mesh size. Without loss of generality, in all calculations, the amplitude of the vibration is equal to one ($M = 1$).

In Fig. 1, a schematic representation of the vibrating pipe is shown. In Fig. 2, predictions of the shear stress versus shear rate in steady shear flow are displayed. At low shear rates $\left(0.001 \leq \dot{\gamma}_0^*(r^*) \leq 0.01\right)$, the fluid presents a Newtonian region, followed by a shear-thinning region and a quasi-plateau at moderate shear rates $\left(0.01 < \dot{\gamma}_0^*(r^*) \leq 10\right)$. Thereafter, the fluid approaches a second Newtonian region at high shear rates $\left(\dot{\gamma}_0^*(r^*) > 10\right)$. Under flow, the system undergoes a transition from a highly structured state (first Newtonian plateau) to a low structured one (second plateau). In the latter, the structure is completely disrupted, and the viscosity value is of the order of the solvent.

It is important to note that the shear stress function is a monotonically increasing function of the shear strain, and its derivative $\dot{\tau}_0 \neq 0$ is always positive. Nevertheless, the second derivative changes sign due to the convexity and concavity of the shear stress function. Insets in Fig. 2 show the corresponding normalized viscosity function and the first normal stress difference versus shear rate in steady shear flow. At low shear rates, the flow presents a region where the viscosity function is constant. At moderate shear rate, the fluid becomes shear thinning, and it tends to a second plateau at high shear rates where the viscosity is lower than that of

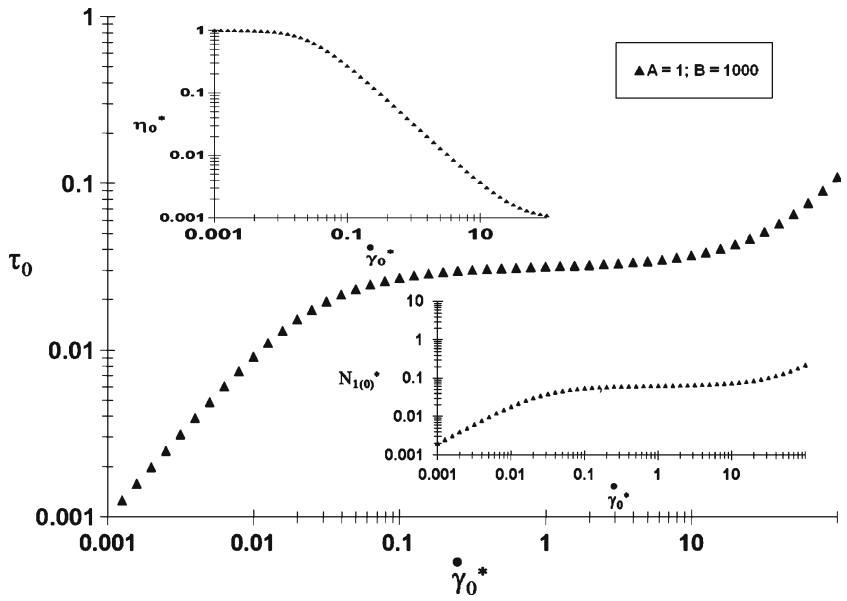

Fig. 2 Dimensionless shear stress versus shear rate. In the *insets*, dimensionless viscosity function and first normal-stress difference versus shear rate. Non-dimensional numbers used in the simulations are $A = 1$, $B = 1{,}000$

the first plateau. On the other hand, the first normal stress difference curve is similar to that of the shear stress.

In Fig. 3, the derivative of the shear stress versus shear strain is plotted. The parameters used in the simulation are $A = 1$ and $B = 1{,}000$. At low shear strains $10^{-3} \leq \dot{\gamma}_0^*(r^*) < 10^{-2}$, the first derivative of the shear stress is almost constant. For moderate values of $\dot{\gamma}_0^*(r^*)\left(10^{-1} \leq \dot{\gamma}_0^*(r^*) < 2\right)$, it decreases monotonically. For $\dot{\gamma}_0^*(r^*) > 2$, the first derivative increases again and the flow enhancement decreases. Notice that the minimum corresponds to the shear-thinning region, where the system undergoes drastic structural changes. In this context, Eqs. 60 and 61 are analytical approximations for the maximum flow enhancement corresponding to the largest structural breakdown.

In Fig. 4, the wall shear rate versus wall stress for various values of the non-dimensional number B (representing various CTAT concentrations) is plotted. At low wall stresses $10^{-3} \leq \tau_w < 10^{-2}$, an almost constant value is predicted, and past a critical wall stress, the wall shear rate increases rapidly $\left(10^{-2} < \tau_w \leq 10^{-1}\right)$. For high wall stresses $\left(\tau_w > 10^{-1}\right)$, the behavior of the wall shear rate is constant throughout. Moreover, the asymptotic value increases as the fluid becomes more shear thinning.

In Fig. 5, the flow enhancement versus wall stress for various values of B is shown ($Re = 0.25$, $We = 0.5$, $A = 0.001$, $\omega^* = 1$). Resonance behavior consisting in a maximum in the flow enhancement is observed at a critical wall stress. The magnitude of this maximum increases, and the curves are shifted to lower wall stresses as the shear-thinning characteristics

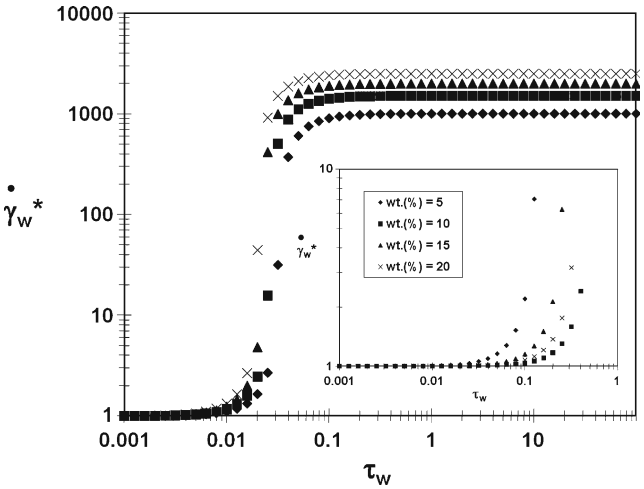

Fig. 4 Dimensionless wall shear rate versus wall stress for various CTAT concentrations. Values of B used in the simulation are 1,000, 1,500, 2,000, 2,500 with $A = 1$. *Inset* Enlargement of the lower wall stress region

of the fluid become predominant. At high wall stress ($\tau_w > 1.2$), all curves become asymptotic to zero flow enhancement. Same result was obtained by Phan-Thien (1978, 1980a, b) and Phan-Thien and Dudek (1982a, b) using several constitutive equations (generalized Newtonian, Tanner strain and strain-rate models) and experimentally observed by Mena et al. (1979).

In Fig. 6, the flow enhancement versus wall stress for various oscillatory Weissenberg numbers is plotted. The parameters used in the mathematical predictions are $Re = 0.25$, $A = 0.001$, $B = 100$, and $\omega^* = 1$. Inset in Fig. 6 shows data for the inelastic case, i.e., $We = 0$, where, for any value of the shear stress, the flow

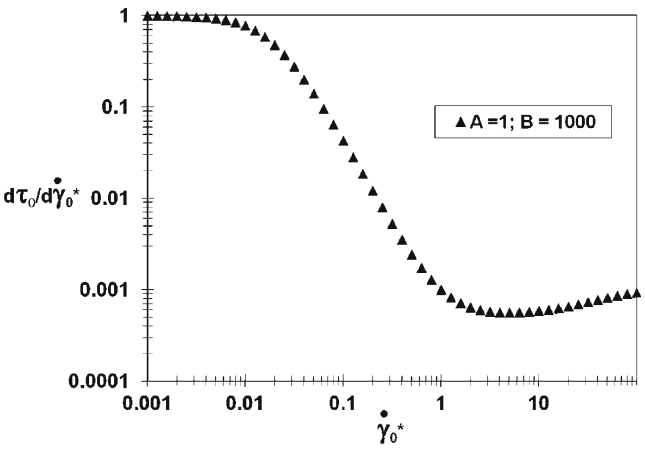

Fig. 3 First derivative of the shear stress versus shear rate. Non-dimensional numbers used in the simulation are $A = 1$, $B = 1{,}000$

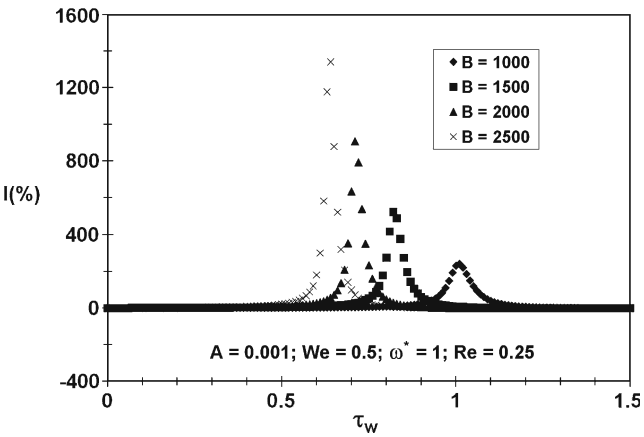

Fig. 5 Flow enhancement versus dimensionless wall stress for various values of B: 1,000, 1,500, 2,000, and 2,500. The dimensionless groups employed in the simulation are $Re = 0.25$, $We = 0.25$, $\omega^* = 1$, and $A = 0.001$

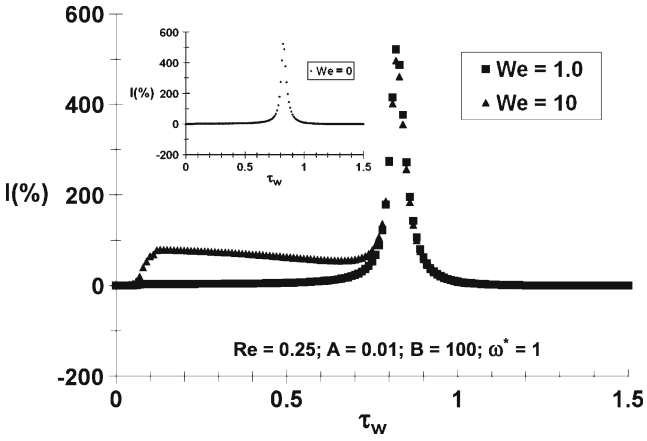

Fig. 6 Flow enhancement versus dimensionless wall stress for various oscillating Weissenberg numbers (*We*): 0.25, 1.0, and 10. *Inset*: inelastic liquid. The dimensionless numbers employed in the simulation are $Re = 0.25$, $A = 0.001$, $B = 1{,}000$, and $\omega^* = 1$

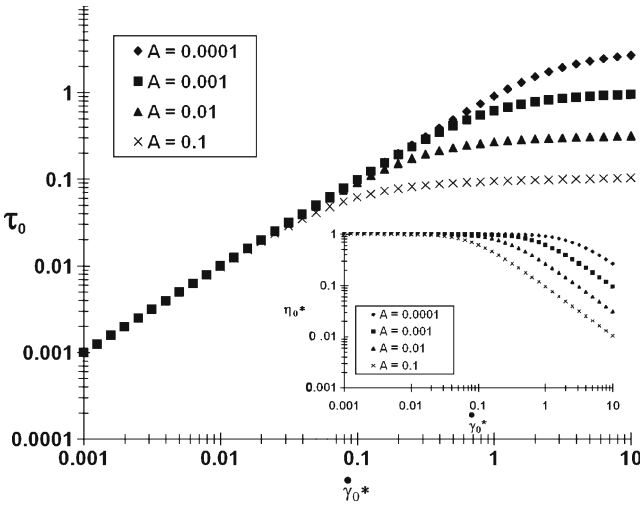

Fig. 7 Dimensionless shear stress versus shear rate for $B = 1{,}000$ and various values of A: 0.0001, 0.001, 0.01, 0.1, and 1. *Inset* Viscosity function versus shear rate

enhancement is always positive and tends to zero for $\tau_w > 0.8$. Nevertheless, when elasticity is present, i.e., $We > 0$, flow enhancement decreases slightly. Mena et al. (1979) and Manero and Walters (1980) reported only positive I (%) values increasing with frequency. The value of the maximum in the flow enhancement I (%) is directly related to the ratio of the upper to lower plateau values of the viscosity, and the effect of the elasticity plays a secondary role in the flow enhancement. A similar conclusion was obtained elsewhere by Phan-Thien (1978, 1980a, b, 1981), Phan-Thien and Dudek (1982a, b), Mena et al. (1979), and Manero and Walters (1980) for several constitutive equations.

It should be noted that this maximum is related to the transition from a more structured fluid into a less structure one (from the shear thinning to second Newtonian plateau regions). The flow enhancement reaches a maximum since the derivative of the stress function in the denominator in Eqs. 60 and 61 attains a minimum value.

Figure 7 shows the zeroth-order shear stress and viscosity function (inset) versus shear rate for several values of the non-dimensional number A (which accounts for the ratio of kinetics of rupture and structure times) at a fixed value of the non-dimensional number B. All curves are monotonically increasing functions of the shear rate. For low values of A, the curves show an extended Newtonian region, whereas high values of A cause the extent of the Newtonian region to decrease. At moderate shear rates, the shear-thinning behavior is observed in all cases (the region where a maximum destruction of structure is achieved). Finally, at high shear rate, the structure is fully disrupted attaining values near the solvent viscosity.

Figures 8 and 9 show the flow enhancement versus wall stress for various values of the non-dimensional number A. The other parameters employed in the simulation are $Re = 0.25$, $We = 0.25$, $\omega^* = 0.25$, and $B = 1{,}000$. To analyze systematically the effect of thixotropy, the value of the kinetic constant is changed to $k = G_0^{-1}$; thus, A becomes the ratio $A = \frac{\eta_0 / G_0}{\lambda}$. When the value of A lies in the range $10^{-4} \leq A < 10^{-2}$ (thixotropy range), the structure does not recover during the deformation period, and hence, the resonance curves are drastically shifted to higher values of the wall stress due to the evolution of the system structure. The magnitude of the maximum increases with the value of A. The shifting implies that, for a thixotropic fluid, the system needs more energy to obtain a change in the volumetric flow rate. In contrast, when the value

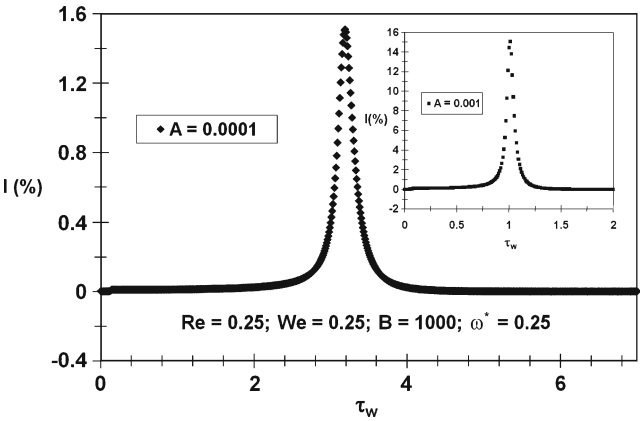

Fig. 8 Flow enhancement versus dimensionless wall stress for $A = 0.0001$ and $A = 0.001$ (*inset*). Non-dimensional numbers used in the simulation are $Re = We = 0.25$, $\omega^* = 0.25$, $B = 1{,}000$

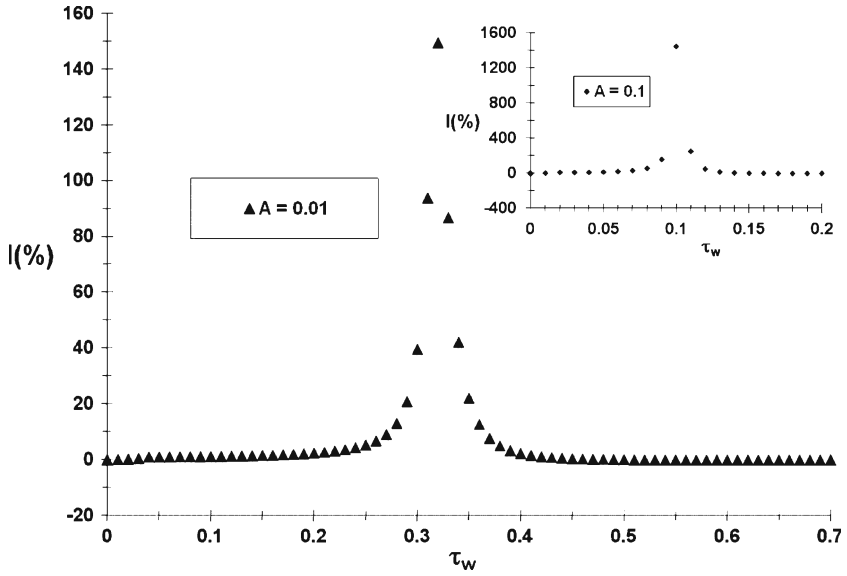

Fig. 9 Flow enhancement versus dimensionless wall stress for $A = 0.01$ and $A = 0.1$ (*inset*). Non-dimensional numbers used in the predictions are $Re = We = 0.25$, $\omega^* = 0.25$, B = 1,000

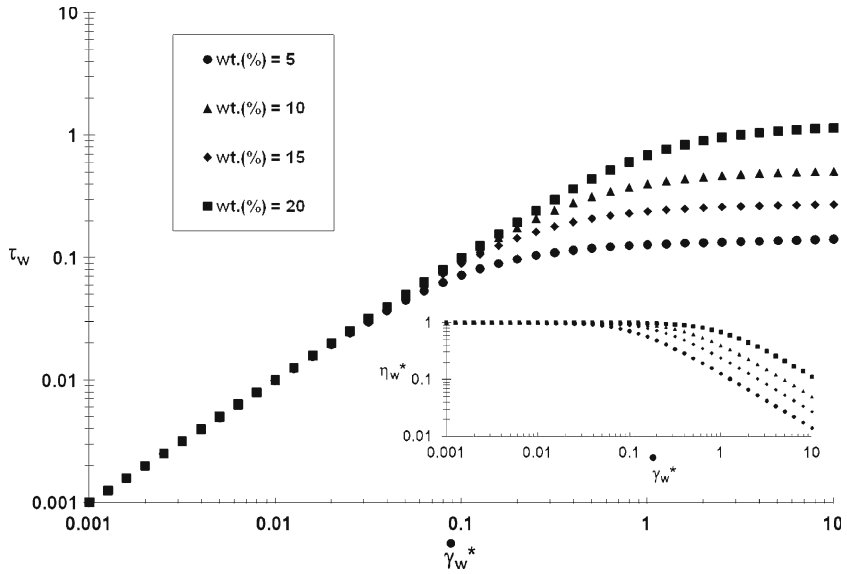

Fig. 10 Dimensionless wall shear stress and wall viscosity function versus wall shear rate for different CTAT solutions. Parameters employed in the simulation are given in Table 1

Table 1 Values of the parameters used in the model as a function of CTAT concentration (Soltero et al. 1999)

C_{CTAT} (wt %)	η_0^{-1} (Pa s)$^{-1}$	η_∞^{-1} (Pa s)$^{-1}$	$k \times 10^{-6}$ (Pa)$^{-1}$	λ (s)	G_0 (Pa)
5	0.0275	19.8	250.0	0.12	41.5
10	0.0061	15.0	30.3	0.33	176.0
15	0.0050	12.6	10.5	0.38	380.0
20	0.0042	12.0	4.2	0.42	620.0

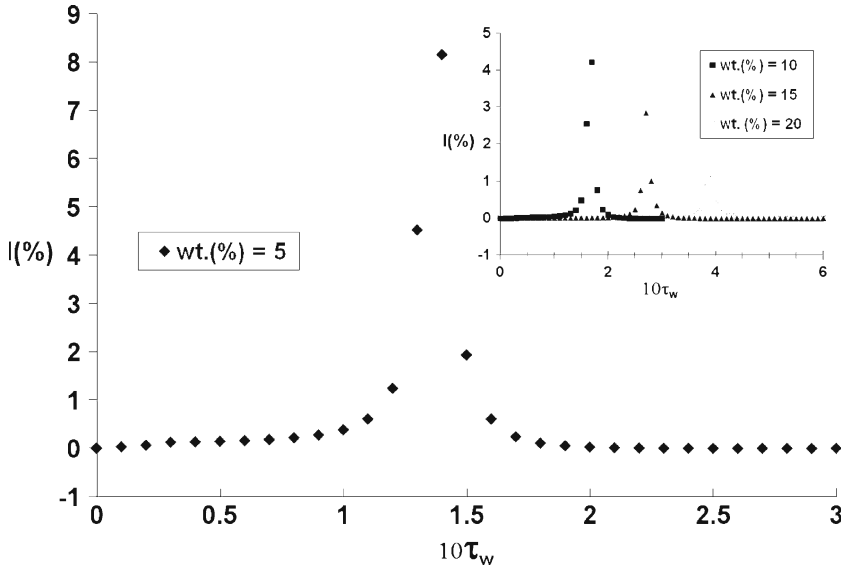

Fig. 11 Flow enhancement versus dimensionless wall stress for a 5 wt% CTAT solution at $T = 30°C$. In the *inset*, 10 wt%, 15 wt%, 20 wt%. Parameters employed in the simulation are given in Table 2

Table 2 Values of the dimensionless number used in the model as a function of CTAT concentration

wt (%)	Re	ω^*	We	A	B	$I_{\max}$	τ_w ($I_{\max}$)
5	0.0688	0.12	0.876	0.076	720	8.15	1.4
10	0.0153	0.33	0.931	0.015	2459	4.42	1.7
15	0.0125	0.38	0.526	0.0055	2520	2.84	2.7
20	0.0105	0.42	0.384	0.0024	2857	1.12	3.9

The parameters employed in the simulation are $\omega = 1.0\,\text{rad/s}$; $a = 5 \times 10^{-2}\text{m}^3$; $\rho = 1,000\,\text{kg/m}^3$ $Re = \frac{\rho\omega a^2}{\eta_0}$; $\omega^* = \omega\lambda$; $We = \frac{\eta_0}{G_0}\omega$; $A = \frac{k\eta_0}{\lambda}$; $B = \frac{\eta_0}{\eta_\infty}$

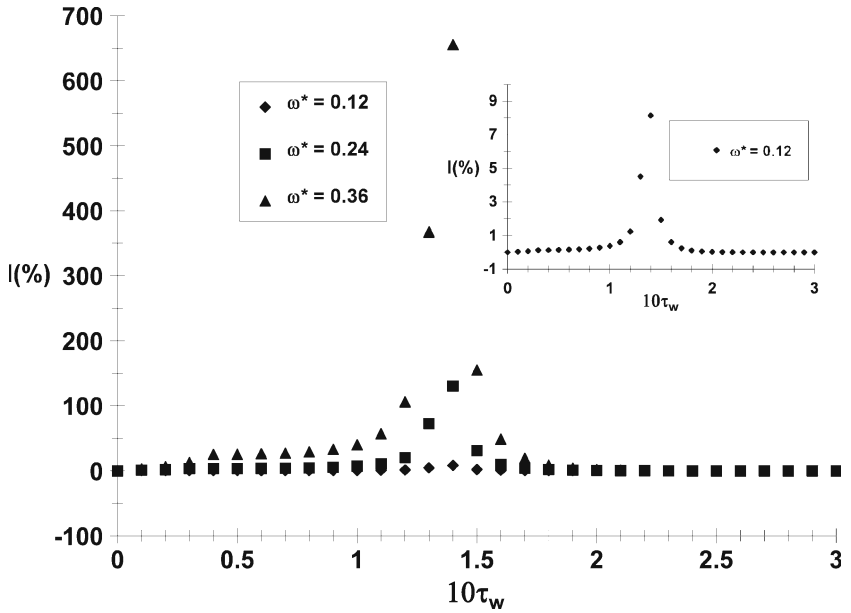

Fig. 12 Flow enhancement versus dimensionless wall stress for a 5 wt% CTAT solution at $T = 30°C$ as a function of the dimensionless frequency. Parameters employed in the simulation are given in Table 3

Table 3 Values of the dimensionless numbers used in the model for several frequencies

wt (%) = 10	β	A	B	De	I_{max}	τ_w (I_{max})
$\omega_1^* = 0.12$	0.573	0.076	720	7.30	8.14	1.4
$\omega_2^* = 0.24$	0.573	0.076	720	7.30	130	1.4
$\omega_3^* = 0.36$	0.573	0.076	720	7.30	656	1.4

Values of the pipe radius and liquid density are $a = 5 \times 10^{-2}\ m^3$; $\rho = 1{,}000\ \mathrm{kg/m^3}$ $\beta = \frac{a^2/\lambda}{\eta_0/\rho}$; $De = \frac{\eta_0/G_0}{\lambda}$; $A = \frac{k\eta_0}{\lambda}$; $B = \frac{\eta_0}{\eta_\infty}$; $0 \leq \omega^* << \omega_c^* = \beta^{-1}$ $\omega_1 = 1\ rad/s$; $\omega_2 = 2\ rad/s$; $\omega_3 = 3\ rad/s$

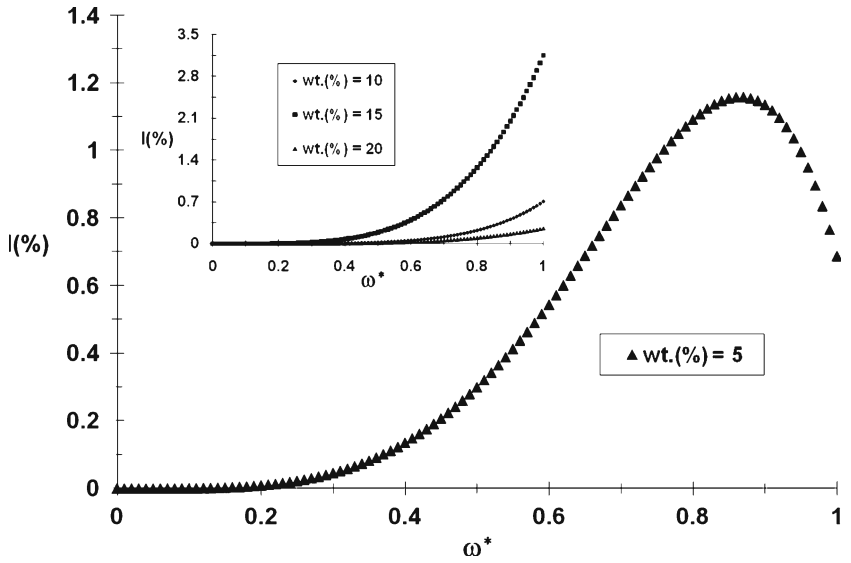

Fig. 13 Flow enhancement versus dimensionless frequency for a 5 wt% CTAT solution at $T = 30°C$ ($\tau_w = 0.23$). In the *inset*, 10 wt%, 15 wt%, and 20 wt%. Dimensionless numbers used in the simulation are given in Table 4

Table 4 Values of the dimensionless numbers used in the model as a function of CTAT concentration

wt (%)	β	A	B	De	τ_w	ω_C^*
5	0.573	0.076	720	7.30	0.23	1.7
10	0.046	0.015	2459	2.82	0.23	21.5
15	0.033	0.0055	2520	1.39	0.23	30
20	0.025	0.0024	2857	0.914	0.23	40

The parameters employed in the simulation are: $a = 5 \times 10^{-2}\mathrm{m}^3$; $\rho = 1{,}000\ \mathrm{kg/m^3}$ $\beta = \frac{a^2/\lambda}{\eta_0/\rho}$; $De = \frac{\eta_0/G_0}{\lambda}$; $A = \frac{k\eta_0}{\lambda}$; $B = \frac{\eta_0}{\eta_\infty}$; $0 \leq \omega^* << \omega_c^* = \beta^{-1}$

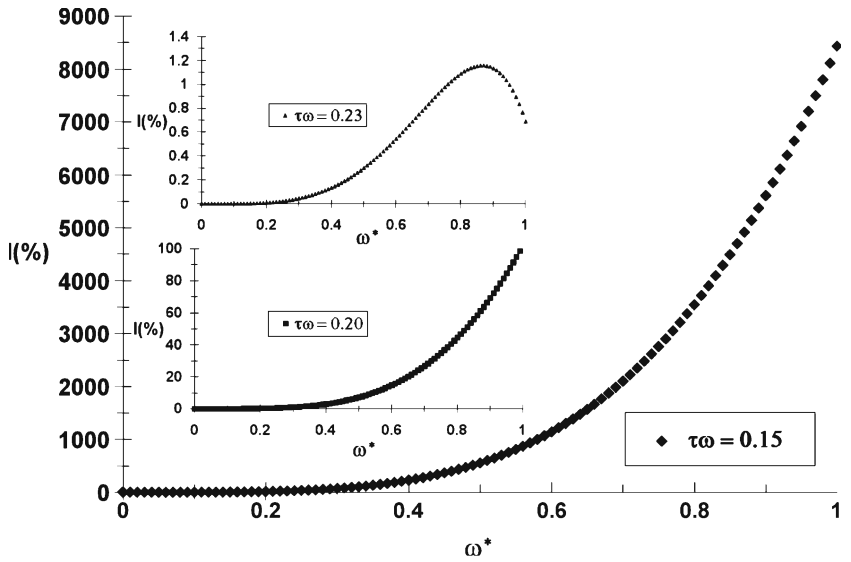

Fig. 14 Flow enhancement versus dimensionless frequency for a 5 wt% CTAT solution at $T = 30°C$ ($\tau_w = 0.15$). In the *insets*, $\tau_w = 0.20$ and 0.23. Non-dimensional numbers used in the simulation are given in Table 4

of A lies in the range $10^{-1} \leq A \leq 10^{0}$ (Fig. 9), the structure recovers quickly, and the curves are shifted to lower wall stresses. Note that the resonance behavior is clearly seen and the maximum in all curves is determined by a coupling between viscoelastic and structural properties in the system.

Predictions of the flow enhancement using wormlike solutions data

Figure 10 displays the zeroth-order shear stress versus shear rate as a function of the CTAT content in the system. The parameters used for this curves are shown in Table 1. Increasing the CTAT content has the effect of enlarging the extent of the Newtonian region, likewise increasing A. The structure of the solution is related to the surfactant content. Inset of this figure shows the corresponding viscosity as a function of the wall shear rate. Again, the shear-thinning slopes have the same value; nevertheless, the viscosity at high shear rate is reported to have different values for each system (Soltero et al. 1999). For low surfactant concentrations (5 wt%), the system needs less energy to be disrupted, which implies that the liquid becomes shear thinning at lower wall stresses.

In Fig. 11, predictions of the flow enhancement (at low frequency) versus wall stress using viscometric data of CTAT for various concentrations at $T = 30°C$ are plotted (Soltero et al. 1999). Parameters employed in the model as functions of CTAT concentration are given in Table 1, and the corresponding dimensionless groups are disclosed in Table 2. For the solution with 5 wt%, the flow enhancement presents at $1.2 < \tau_w < 1.4$ a drastic enhancement with a maximum in the resonance curve of $I(\%) = 8.15$ at $\tau_w = 1.4$. In this region, the fluid experiences a pronounced shear-thinning behavior. The maximum flow enhancement is found in the 5 wt% CTAT content. It has been reported by several authors that the shear thinning effect is the main responsible for the flow enhancement (Phan-Thien 1978, 1980a, b, 1981; Phan-Thien and Dudek 1982a, b; Manero and Mena 1977; Mena et al. 1979; Manero and Walters 1980; Davies et al. 1978; Kazakia and Rivlin 1978, 1979). However, the 5 wt% solution has the smallest B and so the minimum shear-thinning effect (see Table 2). Thixotropy was found to have a negative effect in the flow enhancement, and since the 5 wt% CTAT solution has the largest A value (thixotropy is related to the dimensionless number A, see Table 2), the thixotropy effect is the smallest. The resulting combined effect of shear thinning and thixotropy leads to a maximum flow enhancement at this CTAT solution.

For a CTAT content of 10 wt% (inset in Fig. 11), the maximum in the curve is $I\,(\%) = 4.42$ at $\tau_w = 1.7$. For the 15 wt% solution, the maximum in the curve is $I\,(\%) \approx 2.84$ at $\tau_w = 2.7$, which is lower than that for 10 wt%. Finally, for a CTAT content of 20 wt%, the maximum in the curve is $I\,(\%) = 1.12$ at $\tau_w = 3.9$. The maximum in the curves is shifted to larger wall stresses, implying a larger energy requirement for the flow enhancement.

In Fig. 12, the flow enhancement versus wall stress for a 5 wt% CTAT solution at various frequencies is shown (non-dimensional numbers employed in the predictions are given in Table 3). To quantify the flow enhancement dependence on the frequency, the following ratios are calculated: $\frac{I_{\omega^*=0.24}}{I_{\omega^*=0.12}} = \frac{130}{8.14} \cong 2^4$ and $\frac{I_{\omega^*=0.36}}{I_{\omega^*=0.12}} = \frac{656}{8.14} \cong 3^4$. A relationship between the non-dimensional frequency of the fluid and the flow enhancement follows the form suggested in Eq. 56, when the elastic effects are neglected, namely, $\frac{I_1}{I_0} \cong \left(\frac{\omega_1^*}{\omega_0^*}\right)^4$, where I_0 is the flow enhancement calculated at the dimensional frequency ω_0^* and $\omega_1^* = N^4\omega_0^*$ is a factor of ω_0^* $\left(N \in R^+\right)$. The frequency dependence of the maxima are clearly depicted, contrasting with other results that predict that the flow enhancement is a decreasing function of frequency (Barnes et al. 1971; Davies et al. 1978).

In Fig. 13, the flow enhancement versus frequency for various CTAT solutions is larger in the more diluted solutions. The flow enhancement is predicted to increase with frequency up to a maximum and thereafter it decreases.

Likewise, Fig. 14 shows the flow enhancement versus non-dimensional frequency for a 5 wt% solution and for various wall stresses. It is clear that the flow enhancement is an increasing function of the wall stress and frequency, but in all cases, a maximum is predicted.

Conclusions

In this work, a stochastic perturbation solution of a complex liquid flowing along a vibrating pipe for a general class of noise is presented. The complex liquid was characterized by the BMP equation, which couples a time-dependent equation for the structure changes with the upper-convected Maxwell constitutive equation. The evolution equation for the structural changes was conceived to account for the kinetic process of breakage and reformation of the micelles under flow.

The following conclusions are reached:

- The flow enhancement effect manifests itself as a Re^2 order effect and is only valid in the range of low

frequencies: i.e., $0 \leq \omega^* << \omega_C^*$, where the critical frequency $\left(\omega_C^*\right)$ is determined by a ratio of two transport coefficients. One is associated to the current structure and the other one to the momentum transport.

- The viscoelastic, kinetic, and structural mechanisms in the BMP model were characterized by the association of non-dimensional numbers to each mechanism: (1) $A = \frac{k\eta_0}{\lambda}$ and (2) $B = \frac{\eta_0}{\eta_\infty}$. The first one is associated to the kinetic, viscous, and structural process and the second one to the level of the structure in the system. In particular, when the kinetic constant (k) is $k = G_0^{-1}$, the number A reduces to the Deborah number, which is a measure of the thixotropy effects in the system.
- A necessary condition to obtain a positive flow enhancement in a structural complex liquid is that the system undergoes a transition from a highly structured state into a low structured one.
- The maximum in the curves is closely related to the ratio of viscosities at low and high shear rates and also to a coupling between the kinetics, viscoelastic, structural, and thixotropy effects. The largest flow enhancement was found for low thixotropy (high A value) and low CTAT content.
- Thixotropy was found to have a negative effect in the flow enhancement, i.e., high thixotropy causes low enhancement. In addition, the CTAT content was directly associated to the system thixotropy and the form of the viscosity curve.
- Qualitatively, the flow enhancement for CTAT solution increases with the non-dimensional frequency according to $\frac{I_1}{I_0} \cong \left(\frac{\omega_1^*}{\omega_0^*}\right)^4$ (when the elastic effects are neglected). On the other hand, when the elastic force are dominates, the flow enhancement follows the relationship $\frac{I_1}{I_0} \cong \left(\frac{\omega_1^*}{\omega_0^*}\right)^6$, where I_0 is the flow enhancement calculated at frequency ω_0^* and $\omega_1^* = N\omega_0^*$ $\left(N \in R^+\right)$.

Future work

It would be worthwhile to compare the theoretical predictions with experimental observations, for example, by using viscoelastic surfactants such as CTAT or liquid crystalline suspensions.

Analysis of the effect of oscillating flow on the viscous dissipation in polymer extrusion should be conducted.

One of the most interesting effects of complex fluids is the shear-banding flow. Due to mechanical and thermodynamic instabilities, the system separates in regions of different viscosities. The drastic shear-thinning behavior may produce a very high enhancement in the context of oscillating and pulsating flows.

An energetic advantage is predicted for a liquid with low thixotropy and low CTAT content. It would be desirable to conduct experiments to validate this prediction.

Acknowledgements The authors wish to acknowledge the support of the National Council of Science and Technology of Mexico (CONACYT) Projects 162980 and 100195.

Appendix A

The shear rate to first order in the Reynolds number satisfies the following partial differential equation:

$$\frac{\partial}{\partial t^*}\dot{\gamma}_1^*\left(r^*, t^*\right) = f_1\left(A, B, \dot{\gamma}_0^*\left(r^*\right)\right)\dot{\gamma}_1^*\left(r^*, t^*\right)$$

where $f_1\left(A, B, \dot{\gamma}_0^*\right)$ is given by:

$$f_1\left(A, B, \dot{\gamma}_0^*\right) = \left(\dot{\eta}_0^*\right)^{-1}\left(\left(1 - 2\eta_0^*\right)\dot{\eta}_0^* + A\left(\left(1 - B\eta_0^*\right)\left(\eta_0^*\left(\tau_0\dot{\gamma}_0^*\right)\right) - \frac{1}{2}B\tau_0\dot{\gamma}_0^*\left(\dot{\eta}_0^{*2}\right)\right)\right)$$

The shear rate to second order in the Reynolds number satisfies the following partial differential equation:

$$\frac{\partial}{\partial t^*}\dot{\gamma}_2^*\left(r^*, t^*\right) = f_2\left(A, B, \dot{\gamma}_0^*\left(r^*\right)\right)\dot{\gamma}_2^*\left(r^*, t^*\right) + f_3\left(A, B, De, \dot{\gamma}_0^*\left(r^*\right), t^*\right)$$

where $f_2\left(A, B, \dot{\gamma}_0^*\left(r^*\right)\right)$ y $f_3\left(A, B, De, \dot{\gamma}_0^*\left(r^*\right), t^*\right)$ are given by the next relationship

$$f_2\left(A, B, \dot{\gamma}_0^*\right) = \left(\dot{\eta}_0^*\right)^{-1}\left(\left(1 - 2\eta_0^*\right)\dot{\eta}_0^* + \eta_0^*\left(1 - B\eta_0^*\right)\left(\tau_0\dot{\gamma}_0^*\right) + \tau_0\dot{\gamma}_0^*\left(1 - 2B\eta_0^*\right)\dot{\eta}_0^*\right)$$

$$f_3\left(A, B, De, \dot{\gamma}_0^*, t^*\right) = \left(f_{31}\left(A, B, \dot{\gamma}_0^*\right) + f_{32}\left(A, B, \dot{\gamma}_0^*\right) + f_{33}\left(A, B, \dot{\gamma}_0^*\right)\right) \times f_4\left(A, B, De, \dot{\gamma}_0^*, t^*\right)$$

and $f_{31}\left(A, B, \dot{\gamma}_0^*\right)$; $f_{32}\left(A, B, \dot{\gamma}_0^*\right)$; $f_{33}\left(A, B, \dot{\gamma}_0^*\right)$; $f_4\left(A, B, De, \dot{\gamma}_0^*, t^*\right)$ are defined by:

$$f_{31}\left(A, B, \dot{\gamma}_0^*\right) = A\left(\dot{\eta}_0^*\right)^{-1}\left(\frac{1}{2}\left(1-2\eta_0^*\right)\ddot{\eta}_0^* - \left(\dot{\eta}_0^*\right)^2 + \left(1-2B\eta_0^*\right)\eta_0^*\left(\dot{\tau}_0 + \dot{\gamma}_0^*\frac{\ddot{\tau}_0}{2}\right)\right)$$

$$f_{32}\left(A, B, \dot{\gamma}_0^*\right) = A\left(\dot{\eta}_0^*\right)^{-1}\left(\frac{1}{2}\left(1-2B\eta_0^*\right)\ddot{\eta}_0^* + \tau_0\dot{\gamma}_0^*\left(\dot{\eta}_0^*\right)^2 + \left(1-2B\eta_0^*\right)\left(\tau_0\dot{\gamma}_0^*\right)\dot{\eta}_0^*\right)$$

$$f_{33}\left(A, B, \dot{\gamma}_0^*\right) = -\frac{A}{2}\left(\dot{\eta}_0^*\right)^{-1}\ddot{\eta}_0^* f_{31}\left(A, B, \dot{\gamma}_0^*\right)$$

$$f_4\left(A, B, De, \dot{\gamma}_0^*, t^*\right) = \left(\frac{\tau_0}{\dot{\tau}_0}\left(n\left(\dot{t}^*\right) + De\, n\left(\ddot{t}^*\right)\right)\right)^2$$

Appendix B

$$\left(1 + De\eta_0^*\frac{\partial}{\partial t^*}\right)\tau_2 + De\eta_1^*\frac{\partial}{\partial t^*}\tau_1 = \eta_0^*\dot{\gamma}_2^* + \eta_1^*\dot{\gamma}_1^* + \eta_2^*\dot{\gamma}_0^* \tag{62}$$

Substitution of the following equation

$$\tau_1\left(r^*, t^*\right) = \frac{1}{2}n\left(\dot{t}^*\right)r = \frac{\tau_0}{2\tau_w}n\left(\dot{t}^*\right)r \tag{63}$$

$$\tau_2\left(r^*, t^*\right) = \frac{1}{2}n\left(\ddot{t}^*\right)r = \frac{\tau_0}{2\tau_w}n\left(\ddot{t}^*\right)r \tag{64}$$

$$\eta_1^* = \dot{\gamma}_1^*\dot{\eta}_0^* \tag{65}$$

$$\eta_2^* = \dot{\gamma}_2^*\dot{\eta}_0^* + \frac{1}{2}\dot{\gamma}_1^{*2}\ddot{\eta}_0^* \tag{66}$$

Substitution of Eqs. 63–65, and 66 into Eq. 62

$$\eta_0^*\dot{\gamma}_2^* + \dot{\eta}_0^*\dot{\gamma}_1^{*2} + \left(\dot{\gamma}_2^*\dot{\eta}_0^* + \frac{1}{2}\dot{\gamma}_1^{*2}\ddot{\eta}_0^*\right)\dot{\gamma}_0^* = \frac{\tau_0}{2\tau_w}\left(n\left(\dot{t}^*\right) + De\eta_0^* n\left(\ddot{t}^*\right)\right) + De\frac{\tau_0}{2\tau_w}\dot{\eta}_0^*\dot{\gamma}_1^* \tag{67}$$

Factoring and grouping the above expression

$$\dot{\gamma}_2^*\left(\eta_0^* + \dot{\eta}_0^*\dot{\gamma}_0^*\right) + \dot{\gamma}_1^{*2}\left(\eta_0^* + \ddot{\eta}_0^*\dot{\gamma}_0^*\right) = \frac{\tau_0}{2\tau_w}\left(n\left(\ddot{t}^*\right) + De\eta_0^* n\left(\dddot{t}^*\right)\right) + De\frac{\tau_0}{2\tau_w}\ddot{\eta}_0^*\dot{\gamma}_1^* \tag{68}$$

$$\dot{\gamma}_2^* = -\frac{1}{2}\frac{\ddot{\tau}_0}{\dot{\tau}_0}\dot{\gamma}_1^{*2} + \frac{\tau_0}{2\tau_w}\left(\frac{n\left(\dot{t}^*\right) + De\eta_0^* n\left(\ddot{t}^*\right)}{\dot{\tau}_0}\right) + De\frac{\tau_0}{2\tau_w}\frac{\dot{\eta}_0^*}{\dot{\tau}_0}\dot{\gamma}_1^* n\left(\ddot{t}^*\right) \qquad \dot{\tau}_0 \neq 0 \tag{69}$$

Taking the average of Eq. 69

$$\left\langle\dot{\gamma}_2^*\right\rangle = -\frac{1}{2}\frac{\ddot{\tau}_0}{\dot{\tau}_0}\left\langle\dot{\gamma}_1^{*2}\right\rangle + De\frac{\tau_0}{2\tau_w}\frac{\dot{\eta}_0^*}{\dot{\tau}_0}\left\langle\dot{\gamma}_1^* n\left(\ddot{t}^*\right)\right\rangle \tag{70}$$

and the definitions of shear rate to first order in the Reynolds number

$$\left\langle\dot{\gamma}_1^{*2}\right\rangle = \left(\frac{\tau_0}{2\tau_w\dot{\tau}_0}\right)^2\left\langle\left(n(t^*) + De\, n\left(\dot{t}^*\right)\right)^2\right\rangle = \left(\frac{\tau_0}{2\tau_w\dot{\tau}_0}\right)^2\left(\left\langle n(t^*)^2\right\rangle + De^2\left\langle n\left(\dot{t}^*\right)^2\right\rangle\right) \tag{71}$$

$$\left\langle\dot{\gamma}_1^* n\left(\ddot{t}^*\right)\right\rangle = \left(\frac{\tau_0}{2\tau_w\dot{\tau}_0}\right)^2\left\langle n\left(\ddot{t}^*\right)n\left(\dot{t}^*\right) + De\eta_0^* n\left(\ddot{t}^*\right)^2\right\rangle = \left(\frac{\tau_0}{2\tau_w\dot{\tau}_0}\right)^2 De^2\eta_0^{*2}\left\langle n\left(\ddot{t}^*\right)^2\right\rangle \tag{72}$$

Substitution Eqs. 71 and 72 into Eq. 70, the following equation is obtained:

$$\left\langle\dot{\gamma}_2^*\right\rangle = \frac{1}{2}\left(\frac{1}{2\tau_w}\right)^2\left\{\frac{\left(-\ddot{\tau}_0\right)}{\dot{\tau}_0^3}\tau_0^2\left(\left\langle n\left(\dot{t}^*\right)^2\right\rangle + De^2\eta_0^{*2}\left\langle n\left(\dot{t}^*\right)^2\right\rangle\right) + De^2\tau_0^2\frac{\dot{\eta}_0^{*2}}{\dot{\tau}_0^2}\left\langle n\left(\dot{t}^*\right)^2\right\rangle\right\} \tag{73}$$

In Eq. 73, the relationship $\dot{\eta}_0^{*2} = 2\eta_0^*\dot{\eta}_0^*$ is used. Finally, using the Winner–Kitchen relationship, the following equation is obtained in terms of correlation function:

$$R(0) = \left\langle \left(n\left(\dot{t}^*\right)\right)^2 \right\rangle = \left\langle \left(\left(n\left(\dot{t}^*\right)\right)\right)\overline{\left(\left(n\left(\ddot{t}^*\right)\right)\right)} \right\rangle$$

$$= \int_{-\infty}^{+\infty} \left\langle \alpha^2 dZ(\alpha)\overline{dZ(\alpha)} \right\rangle = \int_{-\infty}^{+\infty} \alpha^2 \Omega(\alpha) d\alpha \qquad (74)$$

$$R_1(0) = \left\langle \left(n\left(\ddot{t}^*\right)\right)^2 \right\rangle = \left\langle \left(n\left(\ddot{t}^*\right)\right)\overline{\left(n\left(\ddot{t}^*\right)\right)} \right\rangle$$

$$= \int_{-\infty}^{+\infty} \alpha^4 \left\langle dZ(\alpha)\overline{dZ(\alpha)} \right\rangle = \int_{-\infty}^{+\infty} \alpha^4 \Omega(\alpha) d\alpha \qquad (75)$$

Hence, Eq. 73 can be rewritten in terms of $R(0)$ and $R_1(0)$

$$\left\langle \dot{\gamma}_2^*\left(r^*, t^*\right) \right\rangle$$

$$= \frac{1}{2}\left(\frac{1}{2\tau_w}\right)^2 \tau_0^2 \left\{ \frac{\left(-\ddot{\tau}_0\right)}{\dot{\tau}_0^3}\left(R_0(0) + De^2\eta_0^{*2}R_1(0)\right) + De^2\frac{\dot{\eta}_0^{*2}}{\dot{\tau}_0^2}R_0(0) \right\} \qquad (76)$$

Equation 76 is an important result given in Eq. 37.

Appendix C

Equation 45 can be simplified integrating by parts the first integral of the numerator

$$I(\%) = \frac{25}{4}M_1^2\omega^{*2}Re^2 \frac{\int_0^{\dot{\gamma}_w^*} \tau_0^4 \left(-\frac{\ddot{\tau}_0}{\dot{\tau}_0^2}\left(1+\omega^{*2}De^2\eta_0^{*2}\right) + \omega^{*2}De^2\frac{\left(\dot{\eta}_0^{*2}\right)}{\dot{\tau}_0}\right) d\dot{\gamma}_0^*(r^*)}{\tau_w^2 \int_0^{\dot{\gamma}_w^*} \dot{\gamma}_0^*(r^*)\, d\left(\frac{1}{3}\tau_0^3\right)} \qquad (77)$$

The first integral can be rewritten as:

$$\int_0^{\dot{\gamma}_w^*} -\frac{\ddot{\tau}_0}{\dot{\tau}_0^2}\tau_0^4\left(1+\omega^{*2}De^2\eta_0^{*2}\right)d\dot{\gamma}_0^*(r^*)$$

$$= \int_0^{\dot{\gamma}_w^*} \tau_0^4\left(1+\omega^{*2}De^2\eta_0^{*2}\right)d\left[\frac{1}{\dot{\tau}_0}\right] \qquad (78)$$

$$u = \tau_0^4\left(1+\omega^{*2}De^2\eta_0^{*2}\right) \Rightarrow$$

$$du = \left\{4\tau_0^3\dot{\tau}_0 + \omega^{*2}De^2\left(\tau_0^4\dot{\eta}_0^{*2} + 4\eta_0^{*2}\tau_0^3\dot{\tau}_0\right)\right\}d\dot{\gamma}_0^* \qquad (79)$$

$$dv = d\left[\frac{1}{\dot{\tau}_0}\right] \Rightarrow v = \frac{1}{\dot{\tau}_0} \qquad (80)$$

Integrating by parts Eq. 78

$$\frac{1}{\dot{\tau}_w}\tau_w^4\left(1+\omega^{*2}De^2\eta_w^{*2}\right) - \int_0^{\dot{\gamma}_w^*} 4\tau_0^3\dot{\tau}_0 d\dot{\gamma}_0^*$$

$$- \omega^{*2}De^2\int_0^{\dot{\gamma}_w^*}\frac{\dot{\eta}_0^{*2}\tau_0^4}{\dot{\tau}_0}d\dot{\gamma}_0^* - \omega^{*2}De^2\int_0^{\dot{\gamma}_w^*}\eta_0^{*2}\tau_0^3 d\dot{\gamma}_0^* \qquad (81)$$

Finally, substitution of Eq. 81 into Eq. 77 and taking $We = \omega^{*2}De^2$ Eq. 46 is obtained

$$I(\%) = \frac{75}{4}M^2\omega^{*2}Re^2 \frac{\tau_w^4 - 4\dot{\tau}_w\int_0^{\dot{\gamma}_w^*}\tau_0^3 d\dot{\gamma}_0^* + We^2\left(\tau_w^4\eta_w^{*2} - 4\dot{\tau}_w\int_0^{\dot{\gamma}_w^*}\eta_0^{*2}\tau_0^3 d\dot{\gamma}_0^*\right)}{\tau_w^2\dot{\tau}_w\left(\dot{\gamma}_w^*\tau_w^3 - \int_0^{\dot{\gamma}_w^*}\tau_0^3 d\dot{\gamma}_0^*\right)} \qquad (82)$$

References

Acierno A, La Mantia FP, Marrucci G, Titomanlio G (1976) A non linear viscoelastic model with structure dependent relaxation times. I. Basic formulation. J Non-Newton Fluid Mech 1:125–146

Barnes HA, Towsend P, Walters K (1969) Flow of non-Newtonian liquids under a varying pressure gradient. Nature 224:585–587

Barnes HA, Towsend P, Walters K (1971) On pulsatile flow of non-Newtonian liquids. Rheol Acta 10:517–527

Bautista F, De Santos JM, Puig JE, Manero O (1999) Understanding thixotropic and antithixotropic behavior of viscoelastic micellar solutions and liquid crystalline dispersions. The model. J Non-Newton Fluid Mech 80:93–113

Bautista F, Soltero JFA, Macias ER, Manero O (2002) On the shear banding flow of wormlike micelles. J Phys Chem, B 106:13018–13026

Bautista F, Soltero JFA, Pérez–López JH, Puig JE, Manero O (2000) On the shear banding flow of elongated micellar solutions. J Non-Newton Fluid Mech 94:57–66

Berret LF (1997) Transient rheology of wormlike micelles. J Rheol 39:725–741

Bird RB, Armstrong RC, Hassager O (1977) Dynamics of polymeric liquids, vol 1. Fluid mechanics. Wiley, New York

Brown JW, Churchill RV (2001) Fourier series and boundary value problems, 6th edn. McGraw Hill, New York

Calderas F, Sánchez-Solis A, Maciel A, Manero O (2009) The transient flow of the PETPEN-Montmorillonite clay nanocomposite. Macromol Symp MACROMEX 2008 (in press)

Casulli J, Clermont JR, Von Ziegler A, Mena B (1990) The oscillating die: a useful concept in polymer extrusion. J Polym Eng Sci 30:1551–1556

Cates ME (1987) Reptation of living polymers: dynamics of entangled polymers in the presence of reversible chain–scission reactions. Macromolecules 20:2289–2296

Cates ME, Candau SJ (1990) Statics and dynamics of worm-like surfactants micelles. J Phys Condens Matter 2:6869–6892

Davies JM, Bhumiratana S, Bird RB (1978) Elastic and inertial effects in pulsatile flow of polymeric liquids in circular tubes. J Non-Newton Fluid Mech 3:237–259

De Andrade Lima LRP, Rey AD (2005) Pulsatile Poiseuille flow of discotic mesophases. Chem Eng Sci 60:6622–6636

De Andrade Lima LRP, Rey AD (2006) Pulsatile flows of Leslie–Ericksen liquid crystals. J Non-Newton Fluid Mech 135: 32–45

De Kee D, Chan Man Fong CF (1994) Rheological properties of structured fluids. Polym Eng Sci 34:438–445

Ding F, Giacomin, Bird RB, Kweon CB (1999) Viscous dissipation with fluid inertia in oscillatory shear flow. J Non-Newton fluid Mech 86:359–374

Dunwoody J (1996) The effects of inertia and infinite amplitude on oscillatory plane shear flow of K-BKZ fluids such as LPDE melts. J Non-Newton Fluid Mech 65:195–200

Edwards MF, Nellist DA, Wilkinson WL (1972) Pulsating flows of non-Newtonian fluids in pipes. Chem Eng Sci 27: 545–553

Fredrickson AG (1964) Principles and applications of rheology. Prentice-Hall, Englewood Cliffs

Gianetto A, Baldi G, Capra V (1973) Laminar pulsed flow of non-Newtonian fluids. Chem Eng Sci 27:295–306

Giesekus H (1966) Die Elastizitat von Flussigkeiten. Rheol Acta 5:29–35

Giesekus H (1982) A simple constitutive equation for polymer fluids based on the concept of deformation-dependent tensorial mobility. J Non-Newton Fluid Mech 11:69–109

Giesekus H (1984) On configuration-dependent generalized Oldroyd derivatives. J Non-Newton Fluid Mech 14:47–65

Giesekus H (1985) Constitutive equation for polymer fluids based on the concept of configuration dependent molecular mobility: a generalized mean-configuration model. J Non-Newton Fluid Mech 17:349–372

Herrera EE (2009) Flujo oscilante de líquidos complejos. Ph.D. thesis, División de Estudios de Posgrado de la Facultad de Química, Universidad Nacional Autónoma de México, Mexico

Herrera-Velarde JR, Mena B (2000) A note on Newtonian and non-Newtonian oscillatory pipe flow. Rev Mex Fis 46(6):566–571

Herrera-Velarde JR, Mena B (2001) Viscous dissipation of a power law fluid in a oscillatory pipe flow. Rev Mex Fis 47 (4):351–356

Herrera Velarde JR, Zenit R, Mena B (2003) Measurement of the temperature rise in non-Newtonian oscillatory pipe flows. J. Non-Newton Fluid Mech 109:157–176

Isayev AI, Wong CM, Zeng X (1990) Flow of thermoplastic in annular die under orthogonal oscillations. J Non-Newton Fluid Mech 34:375–397

Kazakia JY, Rivlin RS (1978) The influence of vibration on Poiseuille flow of non-Newtonian fluids. I. Rheol Acta 18:210–226

Kazakia JY, Rivlin RS (1979) The influence of vibration on Poiseuille flow of non-Newtonian fluids, II. Rheol Acta 18:244–255

Khabakhpasheva EM, Popov VI, Kekalov AN, Mikhailova ES (1989) Pulsating flow of a viscoelastic fluids in tubes. J Non-Newton Fluid Mech 33:289–304

Manero O, Mena B (1977) An interesting effect in non-Newtonian flow in oscillating pipes. Rheol Acta 19:277–284

Manero O, Walters K (1980) On elastic effects in unsteady pipe flows. Rheol Acta 19:277–284

Manero O, Bautista F, Soltero JFA, Puig JE (2002) Dynamics of worm-like micelles: the Cox–Merz rule. J Non-Newton Fluid Mech 106:1–15

Mena B, Manero O, Binding DM (1979) Complex flow of viscoelastic fluids through oscillating pipes. Interesting effects and applications. J Non-Newton Fluid Mech 5: 427–448

Middleman S (1977) Fundamental of polymer processing. McGraw-Hill, New York

Mori N, Wakabayashi K, Horikawa A, Nakamura K (1984) Measurements of pulsating and oscillating flows on non-Newtonian fluids through concentric and eccentric cylinders. Rheol Acta 23:508–513

Phan-Thien N (1978) On pulsating flow of polymeric fluids. J Non-Newton Fluid Mech 4:167–176

Phan-Thien N (1980a) Flow enhancement mechanism of a pulsating flow of non-Newtonian liquids. Rheol Acta 19: 285–290

Phan-Thien N (1980b) The effects of longitudinal vibration on pipe flow of a non-Newtonian fluid. Rheol Acta 19: 539–547

Phan-Thien N (1981) On pulsating flow of a polymer fluids: strain-dependent memory kernels. J Rheol 25(3):293–314

Phan-Thien N (1982) On a pulsating flow of slightly non-Newtonian liquids. J Méc Théor Appl 1:81–89

Phan-Thien N, Dudek J (1982a) Pulsating flow of a plastic fluid. Nature 296:843–844

Phan-Thien N, Dudek J (1982b) Pulsating flow revisited. J Non-Newton Fluid-Mech 11:147–161

Soltero JFA, Puig JE, Manero O (1999) Rheology of cetyltrimethylammonium p-toluenesulfonate–water system. 3. Nonlinear viscoelasticity. Langmuir 15:1604–1612

Spenley NA, Cates ME (1994) Pipe models for entangled fluids under strong shear. Macromolecules 27:3850–3858

Spenley NA, Cates ME, McLeish TCB (1993) Non-linear rheology of wormlike micelles. Phys Rev Lett 71:939–942

Spenley NA, Yuan XF, Cates ME (1996) Non-monotonic constitutive laws and the formation of shear banded flows. J Phys II France 6:551–571

Sundstrom DW, Kaufman A (1977) Pulsating flow of polymeric solutions. Ind Eng Chem Process Dses Dev 16(3):320–325

Townsend P (1973) Numerical solutions of some unsteady flows of elastico-viscous liquids. Rheol Acta 12:13–18

Wong CM, Chen CH, Isayaev AI (1990) Flow of thermoplastic in an annular die under parallel oscillations. Polym Eng Sci 30:1574–1584

Yaglom AM (1965) An introduction to the theory of stationary random functions. Prentice-Hall, Englewood Cliffs (translated by Silverman RA)